Hydrocarbon leakage driven by Quaternary glaciations in the Barents Sea based on 2D basin and petroleum system modeling

Aleksei Kishankov [a,b,*], Pavel Serov [c], Stefan Bünz [c], Henry Patton [c], Alun Lloyd Hubbard [c], Rune Mattingsdal [d], Sunil Vadakkepuliyambatta [c], Karin Andreassen [c]

[a] Gubkin Russian State University of Oil and Gas (National Research University), Leninsky Ave 65, 119991, Moscow, Russia.

[b] Oil and Gas Research Institute of the Russian Academy of Sciences (OGRI RAS), Gubkina Street 3, 119333, Moscow, Russia.

[c] Centre for Arctic Gas Hydrate, Environment and Climate - CAGE, Department of Geosciences, University of Tromsø – the Arctic University of Norway, Dramsveien 201, 9037, Tromsø, Norway.

[d] Norwegian Petroleum Directorate, Storgata 49, 9406, Harstad, Norway.

*** Corresponding author, tel.: +7-911-182-97-64, e-mail address: alexey137k@yandex.ru**

Abstract. The Barents Sea has experienced intense erosion throughout the Cenozoic due to uplift and repeated episodes of glaciation. This, in turn, has driven large pressure and temperature fluctuations in the sediment substrate along with rearrangement of thermogenic oil and gas accumulations. As a result, some hydrocarbon fields have relatively shallow depths, and natural gas release is widespread. This study focuses on the process of hydrocarbon leakage from the Realgrunnen reservoir - encompassing the Hanssen and Wisting discoveries - to the shallow subsurface caused by repeated cycles of glacial erosion in the central Barents Sea throughout the Quaternary. We apply 2D basin and petroleum system modeling to two seismic sections using data from two wells and run ten different scenarios that test model sensitivity to key parameters. We find that the primary factors governing gas leakage are the erosion amount, its distribution between glacial and preglacial stages, and the timing of the glaciations. Our results demonstrate that intense oil and gas leakage from the Realgrunnen reservoir occurs primarily through widespread faults activated during the first deglaciation episode. Further considerable gas leakage occurs by the seal breach after a critical overburden thickness is eroded and pressure on the reservoir decreases to ca. 9 MPa. Modeling reveals that the first deglaciation episode causes up to ca. 20 % loss of oil and gas from the reservoir, whereas leakage after the seal breach yields a further ca. 15 % decrease in gas. Our results are supported by seismic analyses that demonstrate hydrocarbon leakage in the study area.

Key words. Arctic, Barents Sea, hydrocarbon leakage, gas leakage, erosion, glaciations, basin and petroleum system modeling.

1. Introduction

The Barents Sea comprises a large continental shelf bounded by Norway and Russia to the south, the Norwegian Sea in the west, Novaya Zemlya archipelago and the Kara Sea in the east, and the Arctic Ocean in the north. Extensive petroleum exploration and exploitation since the 1960s has confirmed the enormous hydrocarbon potential of the Barents Sea (e.g., Doré, 1995; Spencer et al., 2008; Stoupakova et al., 2011; Gramberg et al., 2000; Lasabuda et al., 2021). The shallow stratigraphic position of petroleum systems has resulted from regional uplift and glacial erosion during the Cenozoic, which removed up to 3 km of overburden substrate (e.g., Henriksen et al., 2011a; Dimakis et al., 1998; Vorren et al., 1991; Nyland et al., 1992; Doré et al., 2000). Furthermore, the complex history of burial and exhumation of hydrocarbon systems across the Barents Sea shelf has greatly influenced the thermal maturation of the source rocks, as well as the compaction, porosity, and permeability of the reservoirs and associated cap-rock seals.

Throughout the Quaternary, at least forty glacial cycles have caused relatively abrupt pressure and temperature fluctuations within the Barents Sea petroleum systems (e.g., Max, Lowrie, 1993; Nøttvedt et al., 1988; Ostanin et al., 2017). These dynamic changes – driven by the episodic advance and retreat of a thick grounded ice sheet across the continental shelf - initiated the redistribution of hydrocarbons within the sedimentary bedrocks through the reactivation of existing faults, with leakage occasionally reaching the seafloor (Chand et al., 2012; Lerche et al., 1997; Vadakkepuliyambatta et al., 2013; Duran et al., 2013; Waage et al., 2019). These glacial cycles also critically controlled the development of gas hydrates - solid ice-like compounds consisting of hydrocarbon gas and water. These form in deposits within the shallow subsurface matrix and remain stable at high pressure and low temperature conditions and will dissociate releasing methane under warming and/or depressurization (Kvenvolden, 1988; Andreassen et al., 2017; Portnov et al., 2016; Serov et al., 2017).

Evidence of gas mobilization and seepage, such as pockmarks, mounds and gas blowout craters (Judd & Hovland, 2007; Andreassen et al., 2017; Bogoyavlensky et al., 2019; 2020), is common across many hydrocarbon-rich regions of the Arctic, particularly on the Barents Sea shelf (Rise et al., 2014, Chand et al., 2012). One remarkable site is located on the northern flank of Bjørnøyrenna (the Bear Island Trough) in the Barents Sea (Solheim and Elverhøi, 1993; Figure 1). Andreassen et al. (2017) report that giant, km-scale craters in this area were formed due to gas hydrate dissociation triggered by the retreat of the Barents Sea ice sheet and subsequent intensive accumulation of free gas in subsurface deposits beneath the remaining gas hydrates. Methane trapped in and below such hydrates is assumed to have migrated to near-surface deposits from deep-seated hydrocarbon reservoirs through faults and vertical focused fluid flow structures, all of which are abundant in this area (Vadakkepuliyambatta et al., 2013; Waage et al., 2020).

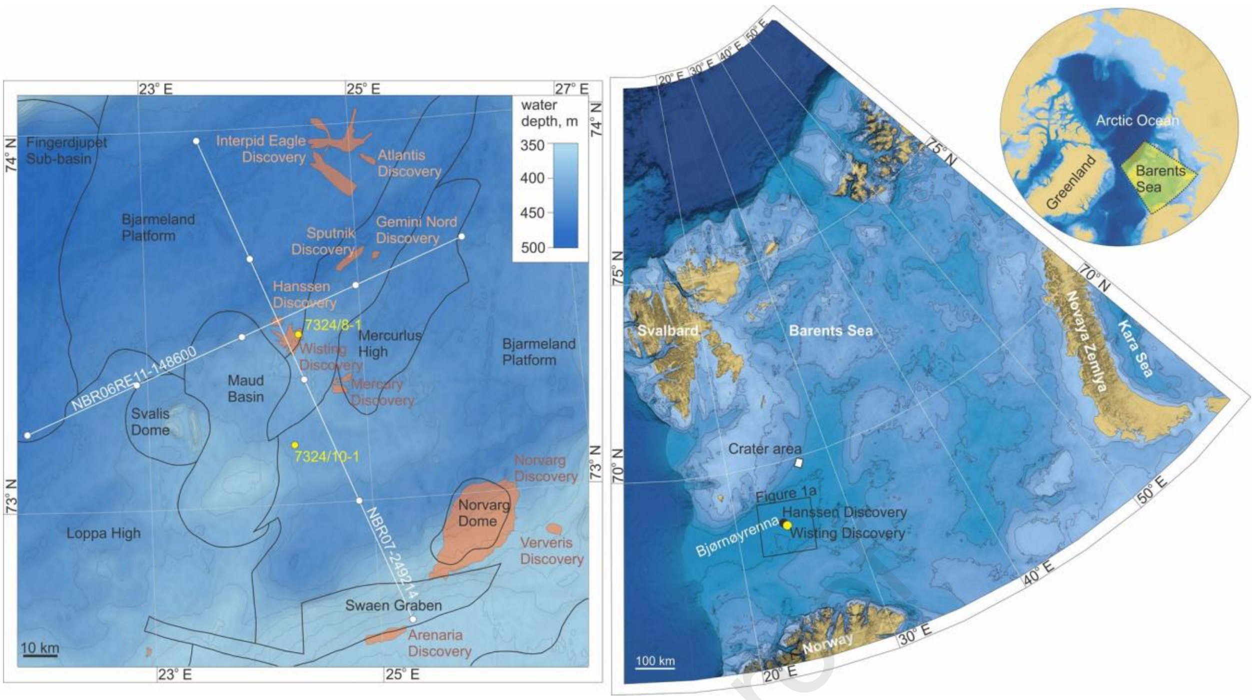

(a) **(b)**

Figure 1. a) Study area and the used data with respect to the regional structural elements. White lines – studied seismic lines, white dots – reference points on seismic lines, yellow dots – studied wells, orange-shaded zones – hydrocarbon discoveries. **b)** Location of the study area and the nearby crater area in the Barents Sea

Different mechanisms control hydrocarbon leakage from reservoirs: faulting or reactivation of existent faults, if they are permeable for fluid migration; breaching of a seal, which occurs when the pressure from accumulated hydrocarbons exceeds the capillary entry pressure of the seal; fracturing of the seal due to overconsolidation, which occurs when the seal is exposed to extensive overburden pressure decrease due to erosion (Cartwright et al., 2007; Hantschel, Kauerauf, 2009; Nygård et al., 2006; Schlömer & Krooss, 1997). For effective trapping of gas or oil, seals must have a high capillary entry pressure and be thick enough to avoid mechanical failure (fracturing and faulting) (e.g., Downey, 1987; Grunau, 1987).

Here, we investigate the mechanisms of hydrocarbon mobilization and leakage from existing petroleum reservoirs to the shallow subsurface during the Quaternary glaciations using 2D basin and petroleum system modeling. We decipher the contribution of the above-described mechanisms to gas loss from reservoirs. Here we focus on Bjørnøyrenna (Figure 1), as this region is characterized by high levels of glacial erosion associated with repeated shelf-edge glaciations (Laberg et al., 2012), and significant changes in pressure and temperature conditions have occurred within the sedimentary cover. Bjørnøyrenna also contains shallow hydrocarbon reserves with the significant Hanssen, Wisting, Intrepid Eagle, Atlantis, Sputnik, Gemini Nord and Mercury discoveries (NPD FactPages), for which potential natural leakage is of environmental and economic relevance. Finally, documented blow-out craters (Andreassen et al., 2017) confirm the potential for large-scale thermogenic methane leakage within the region with a similar geological and glaciological setting.

We design several basin modeling experiments focused on the central part of Bjørnøyrenna, covering two shallow hydrocarbon discoveries – Hanssen and Wisting. A similar approach has been previously used for studying hydrocarbon leakage in the Barents Sea, particularly in the Hammerfest Basin, which hosts several commercial hydrocarbon fields (Duran et al., 2013; Ostanin et al., 2017). However, our model is the first to be forced with a quantitatively constrained glacial chronology spanning the entire Quaternary. Integrating long-term glacial conditions is deemed critical for reconstructing the full history of reservoir leakage as the initial glaciations were likely to have the greatest effect on mobilizing fluids, and, furthermore, the reservoirs are likely to be sensitive to the cumulative impact of repeated glacial episodes.

2. Geological setting

The study area is located at the junction of the Bjarmeland Platform with the Loppa High and the Maud Basin (Figure 1). Generally, the western part of the Barents Sea contains the Caledonian basement, formed as a result of collision between Baltica and Laurentia (Roberts & Gee, 1985). Further evolution of the western Barents Sea involved four major episodes of crustal extension: Late Devonian-Carboniferous, Late Permian, Middle Jurassic-Early Cretaceous and Early Cenozoic (Gac et al., 2018; Faleide et al., 2008). The first episode comprised extension between Greenland and Fennoscandia, resulting in the formation of half-grabens filled with Late Devonian

– Early Carboniferous clastic and carbonate deposits (Dengo & Røssland, 1992). In the Late Carboniferous - Early Permian, the region subsided, experiencing siliciclastic and carbonate sedimentation (Dengo & Røssland, 1992; Roufosse, 1987). The Bjarmeland Platform is inferred to have developed as a stable platform from the Late Carboniferous (Gabrielsen et al., 1990). The second rifting event led to intensive deposition of clastic sediments derived from uplifted areas, such as the Baltic Shield and the Ural belt (Faleide et al., 2015; Glørstad-Clark et al., 2010; 2011). During the Early and Middle Triassic, the Barents Sea shallowed, with the depositional system transitioning from a marine to a continental and deltaic environment (Glørstad-Clark et al., 2011) with sedimentation occurring in progradational sequences (Nøttvedt et al., 1993). In the Late Triassic, the region experienced another episode of subsidence and intensive sediment deposition (Faleide et al., 2008; Nøttvedt et al., 1993). In the Early and Mid-Jurassic, deltaic environments were typical and sea-level rise led to the deposition of marine and, particularly, organic-rich shales. After a third episode of crust extension, new sequences of marine shales were formed from the beginning of Early Cretaceous (Nøttvedt et al., 1993). A fourth rifting episode was connected with the opening of the North Atlantic and Arctic oceans (Dengo & Røssland, 1992) and from the Mid-Oligocene, the area was affected by uplift which led to intensive erosion (Berglund et al., 1986). Throughout the Quaternary, the region experienced over forty glacial cycles (Vorren et al., 1991) characterized by intense glacial erosion, leaving massive accumulations of glacio-marine sediments in trough-mouth fans west and north of the Barents Sea shelf (Reemst et al., 1994; Faleide et al., 1996; Vorren et al., 1988).

Throughout this complex geological evolution, several petroleum systems were initiated within the region. Source rocks exist in a wide stratigraphic range, including the Hekkingen Formation in Upper Jurassic; Snadd, Kobbe and other formations in Triassic; Billefjorden and Tempelfjorden groups in Paleozoic. According to Henriksen et al. (2011b), the most effective petroleum system within the Loppa High and the western part of the Bjarmeland platform is of Triassic origin, corresponding to source rocks of this age. The major reservoirs of the Norwegian sector of the

Barents Sea occur in the interval from Late Triassic to Middle Jurassic. They include Fruholmen, Tubåen, Nordmela and Stø formations, within the Realgrunnen Subgroup of the Kapp Toscana Group, and also the upper part of the Snadd Formation (Dalland et al. 1988; Mørk et al. 1999; NPD Factpages). In platform areas, these reservoirs comprise combined plays, where structural traps are productive on different stratigraphic levels (Henriksen et al., 2011b).

3. Materials and methods

Basin and petroleum system modeling is an important technique widely applied for prospecting and investigating hydrocarbon reservoirs. Effective basin modeling relies on adequate data constraints, including seismic, thermodynamic, geological, petrophysical, glaciological information, for reconstructing processes of sediment deposition, subsidence, compaction, heating (Al-Hajeri, 2009; Hantschel & Kauerauf, 2009; Peters et al., 2012). Petroleum system modeling also requires geochemical data for simulating generation of hydrocarbon in source rocks, and their further migration and accumulation in reservoirs. In this paper, we apply 2D basin and petroleum system modeling across two seismic sections in the central part of Bjørnøyrenna, specifically focusing on the impact of repeated Quaternary glaciations over the past 2.6 Ma on potential hydrocarbon leakage.

Base data for the modeling includes two marine seismic sections from the Norwegian National Data Repository for Petroleum Data (NBR06RE11-148600 and NBR07-249214), crossing at the location of the Hanssen Field, with formation tops and interval velocities from exploration wells 7324/8-1 and 7324/10-1 (Figure 1a). The seismic line NBR07-249214 passes through the Bjarmeland Platform along a north-west to south-east orientation, between the Maud Basin and the Mercurius High, and attaining the Swaen Graben in the south. The line NBR06RE11-148600 is orientated from the south-west to the north-east, crossing the southern part of the Fingerdjupet Sub-basin, the northern part of the Loppa High, the Maud Basin, the Bjarmeland Platform and the

Mercurius High. The 2D models are named according to the shortened names of seismic profiles: NBR07 and NBR06 respectively.

The basin and petroleum system modeling utilized is based on PetroMod 2019 software. The structural basis of a 2D basin model consists of horizons and faults derived from seismic sections interpretation. Other input data for basin modeling include: lithological composition for each layer; periods and amounts of erosion; characteristics of faults – ages, fluid permeability; characteristics of glaciations - chronology, ice sheet thickness; boundary conditions comprised of changing heat flow, water depth, sediment-water interface temperature throughout the geological period of investigation. Input data for petroleum system modeling also include geochemical parameters for each source rock formation – total organic carbon (TOC), hydrogen index (HI), kinetic model of hydrocarbons generation (Al-Hajeri, 2009; Hantschel & Kauerauf, 2009; Peters et al., 2012). There are significant uncertainties for many of the input datasets across the study region. Hence, our approach is to create multiple model experiments describing a range of possible scenarios which allows us to test the sensitivity of results to perturbations in certain parameters.

Some parameters, specifically, amount of erosion, water depth, ice sheet thickness, have sufficient information on their spatial variation, and it is possible to infer their lateral changes along the modeled sections. For this purpose, five equidistant reference points are assigned across each line (Figure 1a). Specific parameter values are set at each reference point, with intermediate values interpolated automatically by PetroMod. However, for many other parameters, lateral variations are neglected and these parameters are assumed to be constant across the study area.

3.1. Seismic data interpretation

Seismic interpretation of the two time-sections was conducted using the Petrel software package (Figure 2). The defined horizons are the Upper Regional Unconformity (URU), Top Hekkingen, Top Snadd, Top Kobbe, Top Klappmys, Top Havert, Top Tempelfjorden and Top Basement. To define the stratigraphic age of seismic horizons, data from wells 7324/8-1 and 7342/10-1 are applied. Also, several faults are defined in both sections. The majority of faults displace Top Hekkingen and Top Snadd horizons, though faults also intersect deeper horizons.

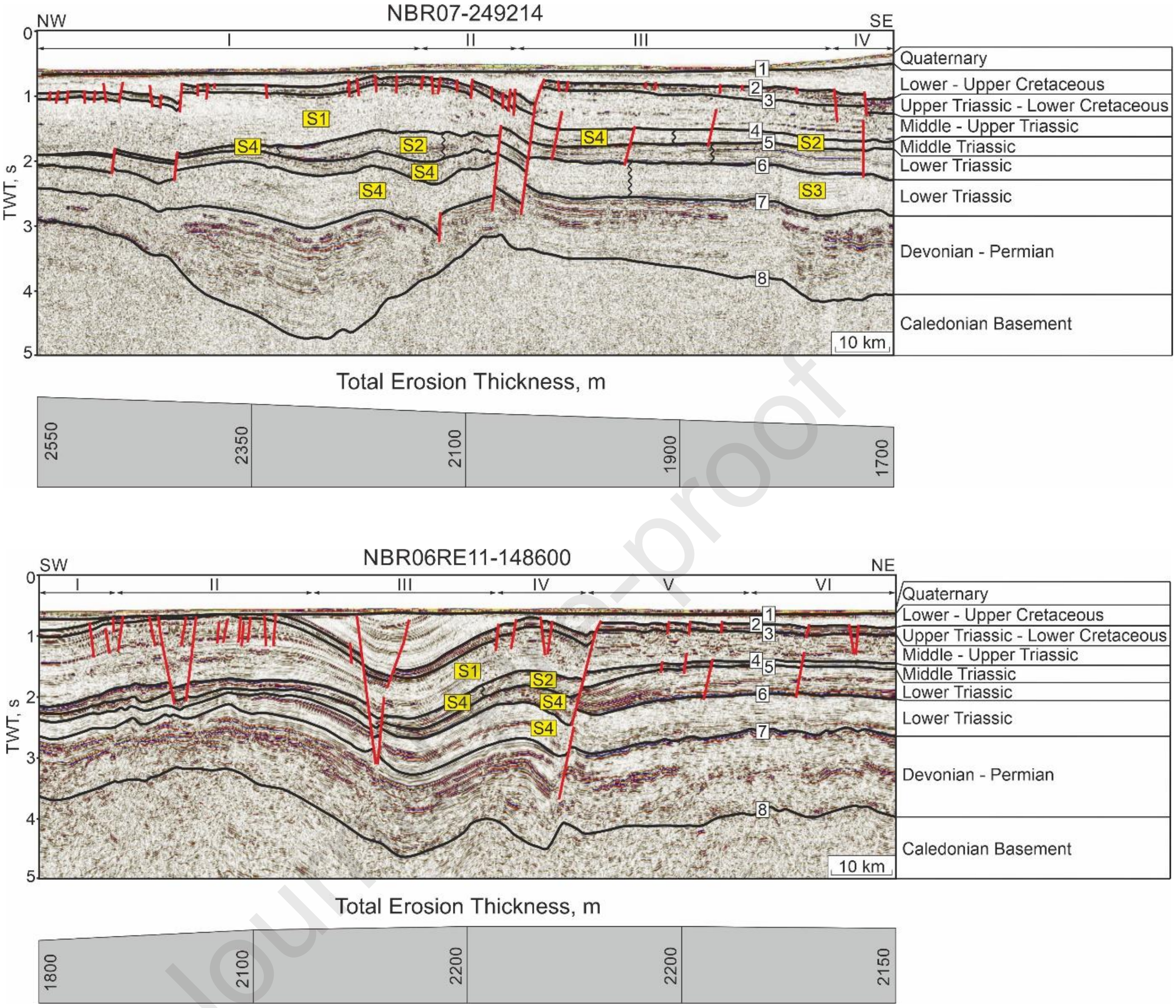

(a)

(b)

Figure 2. Interpreted seismic time sections NBR07-249214 (a) and NBR06RE11-148600 (b). Seismic data courtesy of TGS. Defined horizons (black lines): 1 – URU; 2 – Top Hekkingen; 3 – Top Snadd; 4 – Top Kobbe; 5 – Top Klappmys; 6 – Top Havert; 7 – Top Tempelfjorden; 8 – Top Basement. S1-4 – Source formations (S1 – Snadd, S2 – Kobbe, S3 – Havert, S4 – Steinkobbe). Structural elements (a): I, III – Bjarmeland Platform, II – Hoop Fault Complex, IV – Swaen Graben; (b): I – Fingerdjupet Sub-basin, II – Loppa High, III – Maud Basin, IV – Bjarmeland Platform, V – Hoop Fault Complex, VI – Mercurius High. Red lines represent major faults. Values of total erosion thickness are specified for the reference points based on (Henriksen et al., 2011a). Location of the sections see in Figure 1a.

For the NBR07-249214 seismic section, all structures below Top Hekkingen horizon are intact and remain unaffected by erosion and for NBR06RE11-148600, the northern part of the Loppa

High is eroded. Based on the regional geology (Ohm et al., 2008; Henriksen et al., 2011b; NPD Factpages) and well data, the following sequences are defined between revealed horizons: Nordland Group (Quaternary, above URU), Kolmule-Knurr formations (Lower-Upper Cretaceous between URU and Top Hekkingen), Hekkingen-Fuglen formations and Realgrunnen Subgroup (Middle Jurassic – Lower Cretaceous and Upper Triassic – Middle Jurassic respectively, between Top Hekkingen and Top Snadd), Snadd Formation (Middle-Upper Triassic, between Top Snadd and Top Kobbe), Kobbe Formation (Middle Triassic, between Top Kobbe and Top Klappmys), Klappmys Formation (Lower Triassic, between Top Klappmys and Top Havert) and Havert Formation (Lower Triassic, between Top Havert and Top Tempelfjorden). The Top Basement horizon remains largely unconstrained by the available seismic sections. Hence, the model is restricted from the seafloor extending down to Top Tempelfjorden, thus Billefjorden-Tempelfjorden groups (Devonian – Permian) are not considered in our research. Therefore, with our available base data, we aim to reconstruct the geological history of the study area from the beginning of the Triassic and until the present day.

We further divide the sequence between Top Hekkingen and Top Snadd, to assign the reservoir (Realgrunnen Subgroup) and the overlying seal (Hekkingen-Fuglen formations) (Henriksen et al., 2011b). The relative thickness of these divisions is applied to maintain a proportion of 2:3 respectively (Hekkingen-Fuglen : Realgrunnen), based on nearby well data from the Hanssen and Wisting fields (NPD Factpages). The Stø Formation, which is known to be the major reservoir for many fields of the Barents Sea (NPD Factpages), is not distinguished separately, as it is difficult to define it from the available seismic sections. The Hekkingen-Fuglen layer is defined as a single seal rock for the entire Realgrunnen Reservoir. We also define the distribution of the Steinkobbe Formation, an important regional source formation, as the marine parts of the Kobbe and Klappmys formations (Lundschien et al., 2014; NPD, 2017). For distinguishing the marine environments of deposition of Kobbe and Klappmys, we utilize the paleogeographic maps by

Glørstad-Clark et al. (2010). Marine part of the Havert Formation is considered in our research as equivalent of Steinkobbe, by analogy with overlying layers, deposited in similar settings.

3.2.Main Scenario for basin and petroleum system modeling

For the main reference scenario (Scenario 1), input parameters are assigned with the most plausible values, based on analysis of available data, described below.

3.2.1. Lithology and geochemistry

Lithological composition in the model is assigned according to Norwegian Petroleum Directorate stratigraphic data (NPD Factpages). Lacking detailed information on lithological properties of each formation, all the layers are assigned with shale lithology, except for the Realgrunnen reservoir assigned with the mixture of 50% sandstone and 50% siltstone, and the Quaternary Nordland Group assigned with siltstone lithology. Geochemical parameters for source rocks were assigned according to Abay et al. (2017), where numerous rock samples from different zones of the Barents Sea are studied. Source rocks across the study area include the Snadd, Kobbe, Steinkobbe and Havert formations (Abay et al., 2017; Ohm et al, 2008). Source rock parameters are derived by averaging the corresponding values for the Bjarmeland Platform and the Svalis Dome (Table 1). The Snadd, Kobbe and Havert formations in the study area are characterized by kerogen type III, while Steinkobbe is known to contain kerogen type II (Abay et al., 2017).

We use the classification developed by Pepper & Corvi (1995) available within the used PetroMod software to assign an individual kinetic model for each of the formations. This classification includes five kinetic models associated with organofacies, that define the depositional environments of corresponding source rocks. Based on the available stratigraphic information, the closest match from this classification for Snadd, Kobbe and Havert is organofacies D/E, associated with coastal and ever-wet depositional environments, which is applicable for kerogen type III. The most appropriate option for Steinkobbe is organofacies B, characterized as marine, siliciclastic and applicable for kerogen type II. Lithological and geochemical parameters are assumed to be constant for each formation across the entire section.

Table 1. Geochemical parameters for the source rocks in the study area based on Abay et al. (2017)

Formation	TOC, %	HI, mg HC/g C_{org}	Kinetic model
Snadd	2.71	194	III D/E (Pepper, Corvi, 1995)
Kobbe	1.51	131	III D/E (Pepper, Corvi, 1995)
Havert	0.63	200	III D/E (Pepper, Corvi, 1995)
Steinkobbe	3.72	359	II B (Pepper, Corvi, 1995)

3.2.2. Erosion

The thickness of eroded deposits was assigned to each reference point based on net erosion values for the Barents Sea region (Henriksen et al., 2011a; Figure 2). Total erosive thickness was distributed equally between preglacial and glacial episodes, as one of the possible options (Dimakis et al., 1998). We further assume that glacial erosion is equally distributed between each glacial cycle. The timing of glacial erosion is restricted to the period from 1 to 0 Ma, which is the most probable period of glaciations for the study area according to Knies et al. (2009). The timing of preglacial erosion remains highly uncertain but for the model we assume this period extends from 30 to 15 Ma, following the approximate time of maximum burial of deposits (Duran et al., 2013).

3.2.3. Boundary conditions

Boundary conditions for basin modeling include trends of heat flow, paleo water depth, and the sediment-water interface temperature with respect to time (Hantschel & Kauerauf, 2009).

The heat flow time-series is assigned with peaks corresponding to the main crustal extension events described above, including Late Permian, Middle Jurassic – Early Cretaceous and Early Cenozoic, which must affect deposits considered in our model. Assuming a common geological history for the SW Barents Sea, the peaks of the crustal extension events are assigned according to Duran et al. (2013) for the Hammerfest Basin. The background value is assigned 60 mW/m^2, which is equal to the present-day value (Pascal et al., 2010).

Paleo water depths are determined at each reference point according to the paleo-bathymetric maps of Smelror et al. (2009). Sediment-water interface temperature trends are defined with respect to paleo-geographic environments also at each reference point. For subaerial periods, temperatures are defined using an automatic function, based on paleo-surface temperatures for the given latitude and region of the world (73-74°N, Europe), with respect to a paleo-location model of the region (Wygrala, 1989). For submarine periods, temperatures are assigned a constant value of 2°C according to the World Ocean Database (Boyer et al., 2018).

3.2.4. Glaciations

Multiple, shelf-wide glaciations impacted the study area from 1 Ma through to the Holocene though the region experienced generally less-extensive glacial activity and associated erosion from 2.4 up until 1.0 Ma (Knies et al., 2009).

Data on the timing of glacial cycles, including episodes of ice sheet growth, retreat, and interglacials are extracted for each reference point of the seismic lines using the Last Glacial Maximum ice sheet reconstruction by Patton et al. (2016, 2017) (UiT ice sheet model (ISM)), expanded to cover the last 0.12 Ma and resolve three glacial episodes: the Early, Mid and Late Weichselian. To define the timing of glaciations throughout Quaternary prior to 0.12 Ma, we apply the marine $\delta^{18}O$ isotope stack of Lisiecki & Raymo (2005). Following a simplistic approach, we use a threshold value of 3.75 ‰ $\delta^{18}O$ to distinguish glacial from interglacial conditions (e.g., Fabel et al., 2002; Figure 3).

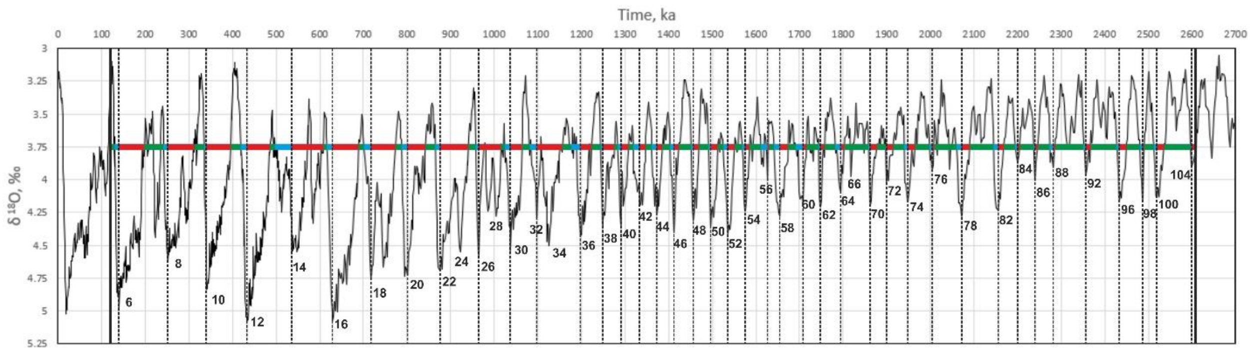

Figure 3. Fragment of the $\delta^{18}O$ stack (Lisiecki, Raymo, 2005) from ca. 2.6 Ma to 0.12 Ma interpreted with respect to glacial cycles, assuming threshold value of 3.75 ‰ $\delta^{18}O$. Red intervals – ice growth, blue intervals – ice retreat, green intervals – interglacials, dashed black lines – maximum of ice growth. Numbers mark marine isotope stages corresponding to maximum ice sheets distribution.

From 1 Ma to present, 13 glacial cycles are defined, including those with a well constrained ice sheet model from 0.12 Ma to 10 ka. For the entire Quaternary period, from 2.6 Ma to present, 44 individual glacial cycles are defined (Appendix A). For Scenario 1, only the last 1 Ma are considered (Figure 4). Maximum ice thickness for glacial cycles from 0.12 Ma are extracted for each reference point from the UiT-ISM (Patton et al., 2016; 2017). Maximum ice thickness for previous glacials (1 - 0.12 Ma) are back-interpolated from the Early Weichselian using data from the UiT-ISM.

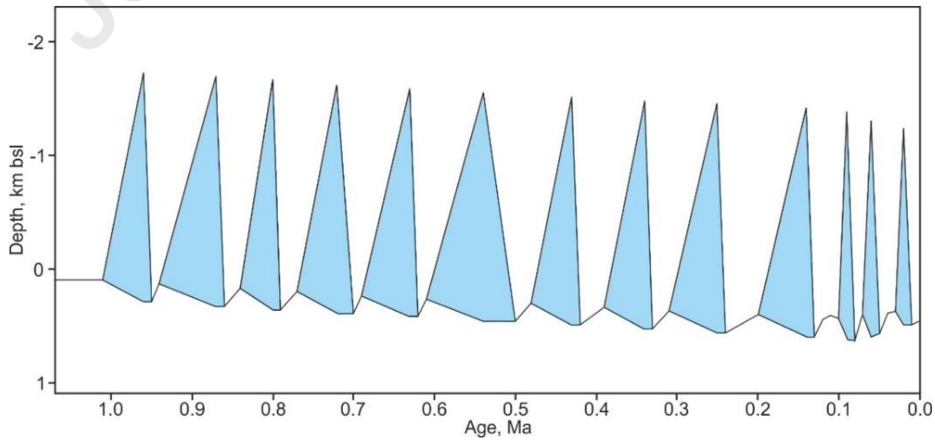

Figure 4. Glacial cycles assigned in Scenario 1.

3.2.5. Faults

Faults are important conduits for promoting fluid migration from thermogenic hydrocarbon reservoirs (Hantschel, Kauerauf, 2009; Chapman, 1983). Faults can either be conductive (open) or non-conductive (closed) to fluid-flow, and this property can vary during the geological history of a sedimentary basin. Following Ostanin et al. (2017), we assume that during the Quaternary faults were open during ice retreat, due to decreasing overburden pressure, and closed during phases of ice sheet growth as well as interglacials. Hence, for the 13 glacial cycles, the assigned permeability history consists of 27 distinct episodes (Appendix B1). The permeability history is manually assigned for each fault, crossing the Hekkingen-Fuglen layer, acting as a seal for the Realgrunnen reservoir. Based on seismic interpretation, there are 39 faults crossing the Hekkingen-Fuglen layer in the NBR07-249214 section. Faults might also be open during interglacials, however we do not investigate this scenario because no abrupt pressure decrease forcing intensive upward fluid migration occurs during interglacials. Nevertheless, interglacial periods might contribute to less active "background" leakage not reflected in our model.

3.3. Additional scenarios

To investigate the sensitivity of our basin model, nine more scenarios are considered, involving perturbations to the key parameters of heat flow, source rock generation potential, glacial loading, and fault permeability (Table 2).

Table 2. Summary of scenarios for sensitivity analysis

Scenario No.	Changes to the Main Scenario (No. 1)
2	Heat flow increased by 10%
3	Heat flow decreased by 10%
4	TOC increased by 2 times
5	Maximum ice sheet thickness (1-0.12 Ma) increased by 20%
6	Maximum ice sheet thickness (1-0.12 Ma) decreased by 20%
7	Faults are closed for fluids
8	Total erosion thickness divided in proportion 1:2 (preglacial:glacial)

9	Total erosion thickness divided in proportion 2:1 (preglacial:glacial)
10	Glacial cycles start from the beginning of the Quaternary

Scenarios 2 and 3 investigate intensity of hydrocarbon generation and subsequent accumulation in the reservoir by increasing and decreasing heat flow by 10% of the background value (60 mW/m^2), respectively. These changes impact the thermal maturation of the source rocks. In Scenario 4, the TOC content of each source rock is doubled, governing the potential quantity of hydrocarbons generated in the model.

Scenarios 5 and 6 account for ice sheet thickness uncertainties and their impact on pressure fluctuations in the Realgrunnen reservoir, where maximum ice sheet thickness from 1 to 0.12 Ma is increased and decreased by 20%, respectively. Scenario 7 investigates fault properties during the region's geological history. Here, all faults are considered closed during glaciations, regardless of whether the sedimentary basin experienced ice-sheet-induced pressure variations which govern the amount and timing of hydrocarbon leakage.

Scenarios 8 and 9 invoke changes in the temporal distribution of erosion between preglacial and glacial periods. In Scenario 8, the thickness of deposits eroded during the preglacial period is considered half that of deposits eroded during glacials, i.e., net erosion is divided in proportion 1:2. In Scenario 9, preglacial erosion is assumed to be more intensive, with net erosion divided in proportion 2:1. Scenario 10 extends the model simulation to a time-scale before 1 Ma. It is supposed that glaciations covered the study area from the beginning of Quaternary, rather than from 1 Ma until present. Hence, we assign all glacial cycles from 2.6 Ma to present, interpolated on the basis of $\delta^{18}O$ curve (Lisiecki & Raymo, 2005; Figure 3).

Based on published paleo-reconstructions of the Northern Hemisphere ice sheets (Batchelor et al., 2019), prior to the Quaternary (i.e., the Gauss Chron 3.59 - 2.6 Ma), Bjørnøyrenna was completely ice free. Knies et al. (2009) propose that Bjørnøyrenna experienced intensive, shelf-wide glaciations from 1 Ma through to the Holocene, yet from 2.4 to 1 Ma, less extensive glacial episodes also occurred. Hence, for Scenario 10, we infer that the thickness of the Barents Sea ice sheets gradually increased with each subsequent glaciation from the onset of the Quaternary until 1 Ma (Figure 5).

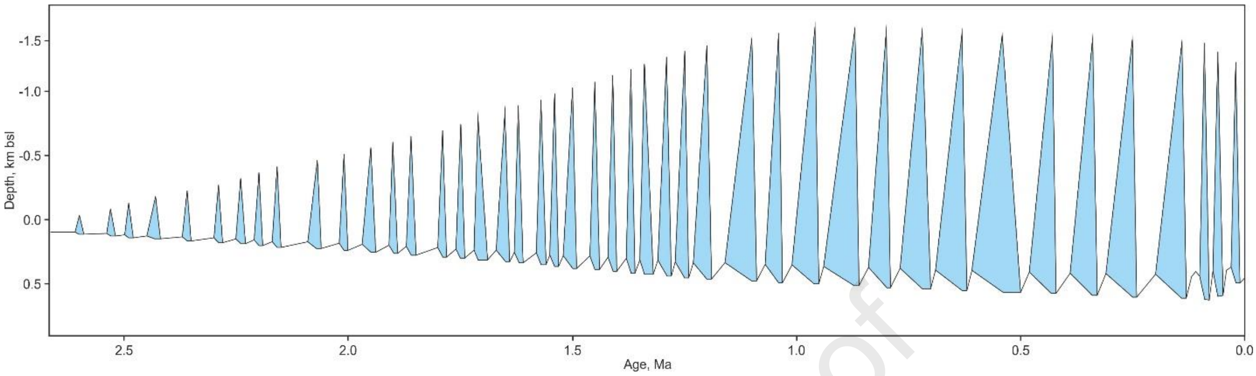

Figure 5. Glacial cycles assigned in Scenario 10

As Scenario 10 involves additional glaciations before 1 Ma, the history of faults permeabilities also needs to be complemented. For each fault, crossing the Hekkingen-Fuglen layer, additional periods of activity are assigned. It is assumed that during the entire Quaternary faults were open during ice retreat and closed during other time periods, the same as for the period from 1 till 0 Ma in the main scenario. New permeability history in Scenario 10 consists of 89 periods (Appendix B2).

4. Results

All the described scenarios are implemented for the NBR07 model. Hydrocarbon migration for all the scenarios is applied by the flowpath method, which is only buoyancy-driven and is neglecting timing and lateral migration in low-permeable layers (Hantschel, Kauerauf, 2009).

4.1. Comparison of different scenarios

The model demonstrates thermal maturation as revealed by vitrinite reflectance (Figure 6) which differs for separate layers with the source rocks (Snadd, Kobbe, Klappmys, Havert). Thermal maturation is determined according to the Easy%Ro model, proposed by Sweeney & Burnham (1990).

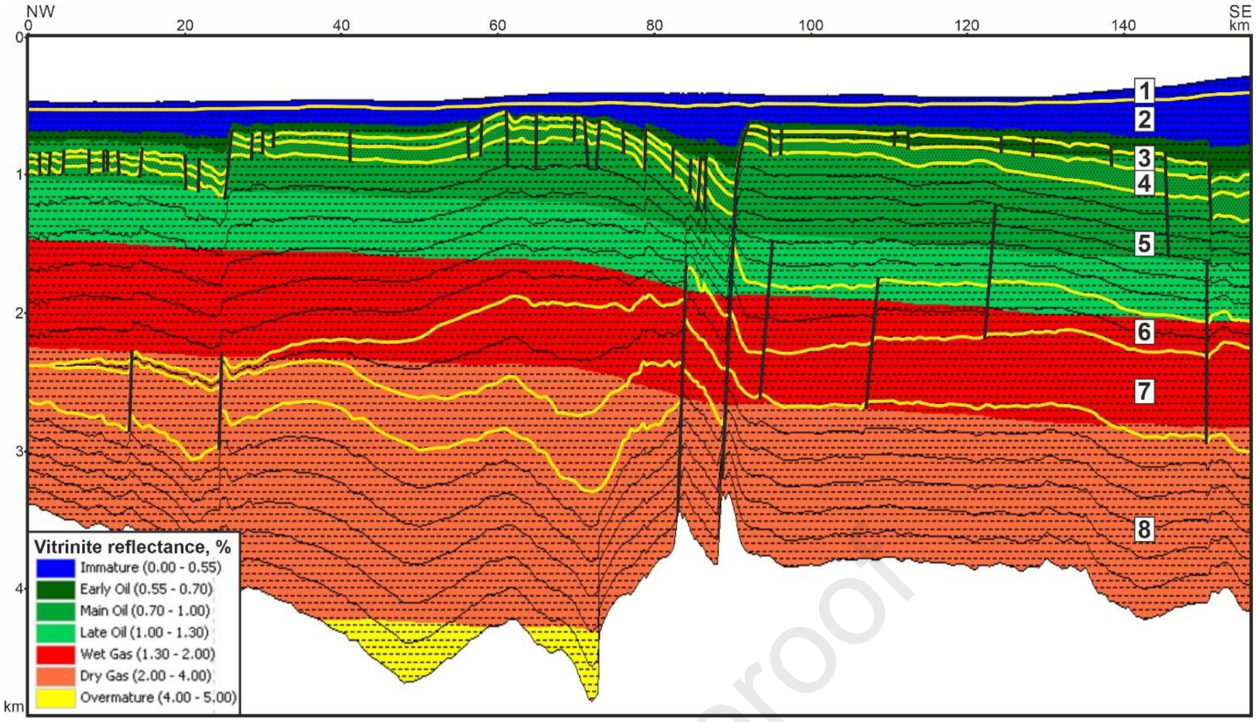

Figure 6. Simulated section exhibiting present-day thermal maturation by values of vitrinite reflectance for the NBR07 model (Scenario 1). Layers in the section: 1 – Nordland Group, 2 – Kolmule-Knurr formations, 3 – Hekkingen-Fuglen formations, 4 – Realgrunnen Subgroup, 5 – Snadd Formation, 6 – Kobbe Formation, 7 – Klappmys Formation, 8 – Havert Formation.

Hydrocarbon accumulation in the Realgrunnen reservoir initiates at ca. 160 Ma (Figure 7A, B). The first gas leakage occurs from 30 to 15 Ma associated with uplift and preglacial erosion (Figure 7A), whereas oil does not show significant loss at this period. Additional minor accumulation of gas occurs after uplift, and a period of intense leakage driven by glaciations starts for both oil and gas from 0.96 Ma onwards. The largest amount of gas is lost during pre-glacial erosion. Certainly, gas leaks due to the seal breach by pressure from the accumulated hydrocarbons, as we do not assign faults open in this period. This process, however, is beyond the scope of our work, which concentrates on leakage driven by Quaternary glaciations.

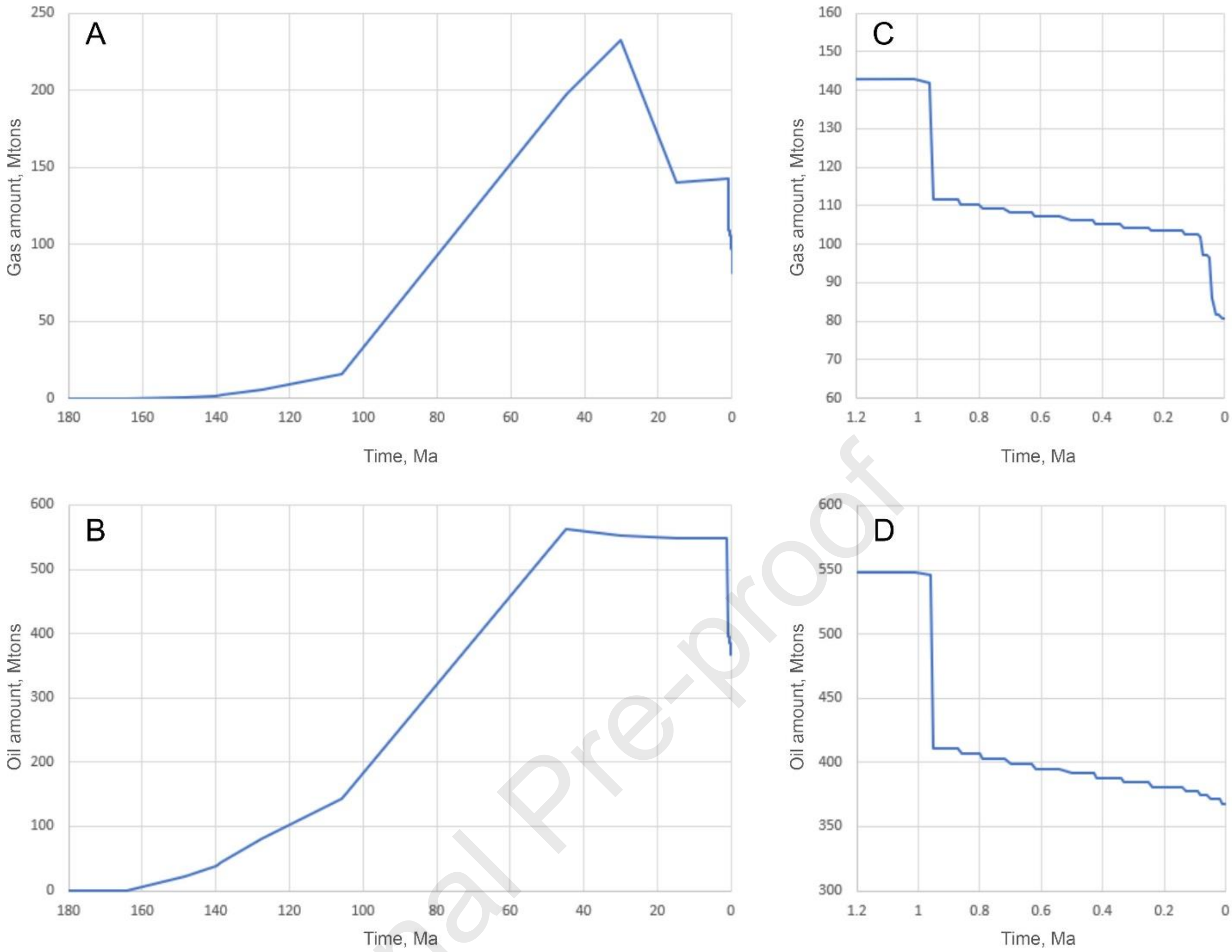

Figure 7. Graphs of gas (A) and oil (B) amount in the Realgrunnen reservoir during geological history with scaled-up fragments for the period of glaciations (C, D) (Scenario 1)

A similar pattern of glacial-driven leakage occurs for model scenarios 1 – 6 (Figure 8). Initially, an abrupt phase of leakage commences from 0.96 to 0.95 Ma, coeval with the first episode of deglaciation and fault opening. The leakage amount associated with Scenarios 1 – 6 during this phase is between 19.2 and 22.4 % of gas and between 17.6 and 25.5 % of oil, both accumulated prior to the first glacial cycle. Episodic, but less intensive leakage continues during subsequent episodes of ice sheet retreat when faults are open and conductive. The next phases of intense leakage are observed for gas from 0.08 to 0.07 Ma and from 0.05 to 0.04 Ma, corresponding to interglacial periods when there are no glacial loading and additional overburden pressure. In Scenario 7, when faults are specified to be non-conductive, gas leakage occurs exclusively in these periods, apparently, by breach of the seal due to pressure from hydrocarbons accumulated within the reservoir. Likewise, we infer this is a common mechanism to Scenarios 1 – 6 from 0.08 Ma onwards where intense leakage occurs due to seal failure, rather than fluid flow via faults. During the final interglacial period 0.01-0.00 Ma (corresponding to the Holocene), leakage does not occur. The gas volume within the reservoir during this period must be small and insufficient to generate enough pressure for triggering the seal breach. Leakage after the seal breach occurs from 0.08 Ma onwards under Scenarios 1 – 6, at a level of between 11.9 and 15.8 % of gas accumulated by the first glacial cycle. On the contrary, oil in Scenarios 1 – 6 does not leak by breach of the seal at any period (Figure 8B). During the whole glaciation time, it escapes the reservoir only through faults when they are considered open. Total leakage over the entire glacial period from 1.0 Ma onwards is 38.5-44.4 % of the net gas existing by the beginning of glaciations and 26.0-33.2 % of the net oil.

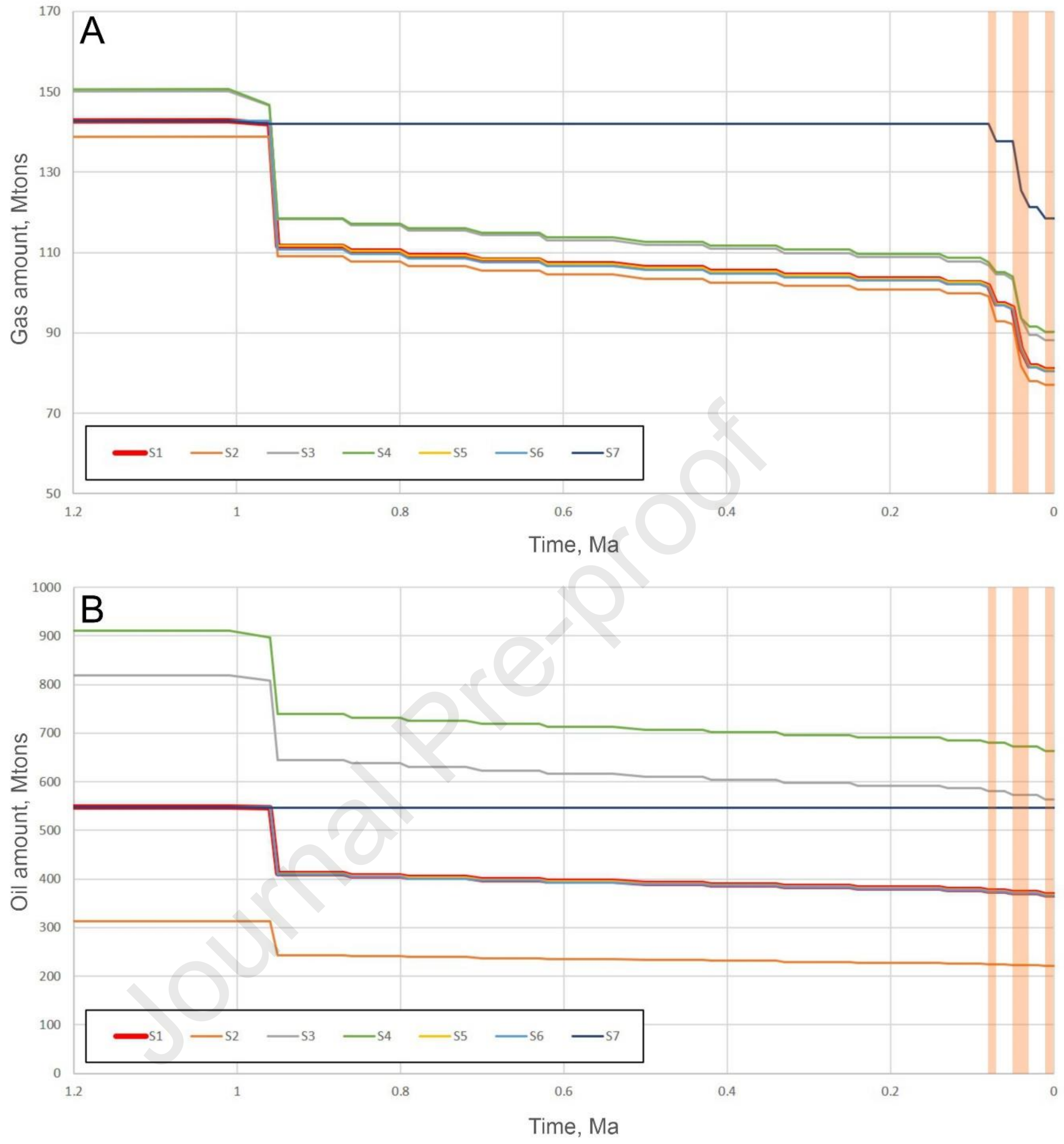

Figure 8. Graph of gas (A) and oil (B) amount in Realgrunnen from 1.2 till 0 Ma (S1-7 – Scenarios 1-7). Orange transparent intervals – interglacials after 0.08 Ma

At the beginning of the proposed seal breach by gas (time stage 0.08 Ma), the minimum thickness of rocks is ca. 290 m, with an additional water column of 620 m, which yields a hydrostatic pressure of ca. 9.1 MPa on the reservoir. Thus, when glacial erosion reduces the thickness of overlying rocks to critically small values, gas can no longer be trapped properly in the shallow reservoir of Realgrunnen, and subsequently starts to leak through the seal due to exceeding gas pressure in the reservoir over capillary entry pressure of the seal.

Scenarios 8 and 9 with their different amounts of preglacial and glacial erosion, likewise yield contrasting gas leakage histories (Figure 9A, C). In Scenario 8, less gas leaks during preglacial phases of uplift (30-15 Ma) and more gas subsequently accumulates (15-0.96 Ma), as the source rocks remain buried deeper and there is greater hydrocarbon generation compared to Scenario 1. Scenario 9 yields the contrary situation. Leakage due to glacial action occurs in a similar manner for Scenarios 1, 8, 9, as well as for Scenarios 1-6 (Figure 8). However, in Scenario 8, leakage by the seal breach starts earlier (Figure 9C), when hydrostatic pressure on the reservoir decreases to 10.4 MPa, due to the larger quantity of trapped fluid creating higher pressures on the seal. The opposite is observed in Scenario 9, where the seal breach does not occur almost at all, probably, due to the small quantity of gas. During the first glacial cycle, 20.4 % of gas leaks in Scenario 8 and 23.9 % in Scenario 9; after the seal breakdown 26.2 % is lost in Scenario 8. As for oil, Scenarios 8 and 9 do not show considerable differences from Scenario 1 (Figure 9B, D). Total loss for the entire period of glaciations is 32.8-52.5 % of gas accumulated by the first glacial cycle and 32.7-33.7 % of oil.

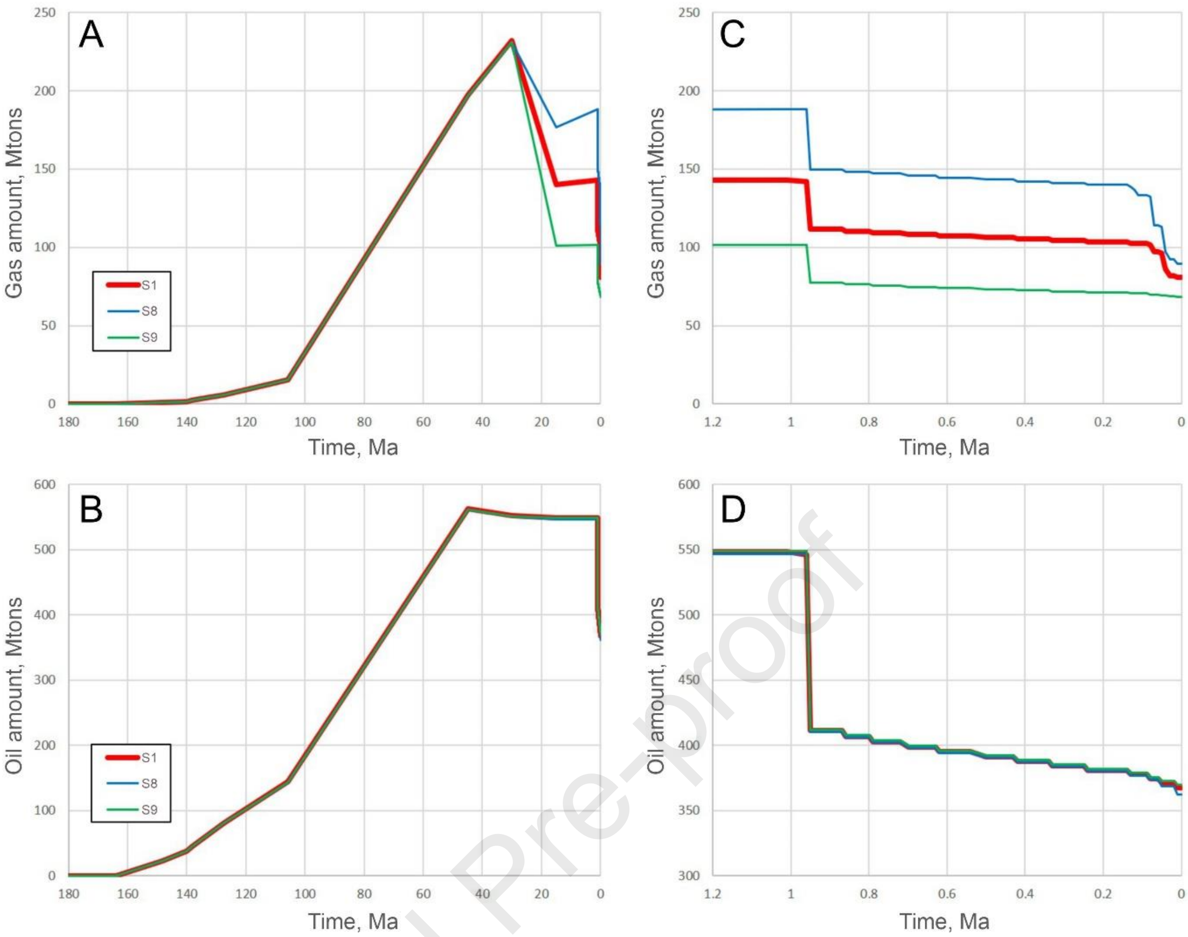

Figure 9. Graph of gas (A) and oil (B) amount in Realgrunnen during geological history (a) with scaled-up fragments for the period of glaciations (C, D) (S1,8,9 – Scenarios 1, 8, 9)

Scenario 10, where glacial erosion starts from the first assigned cycle at 2.6 Ma, unsurprisingly results in a markedly different pattern of leakage (Figure 10). The onset of the first significant leakage is earlier, due to the first phase of open faults during the first assigned deglaciation (2.6-2.59 Ma) which results in 23.7 % of gas and 26.8 % of oil loss. Slow leakage through open faults then occurs coincident with periods of ice retreat. Further gas leakage due to the seal breach also commences earlier, from 0.24 Ma, to remove 16.7 % of gas accumulated by the first glacial cycle. This happens as the critical thickness of the overlying rocks for the seal breach occurs earlier than in Scenario 1. Total loss over the entire glacial period is 58.0 % of gas and 46.3 % of oil.

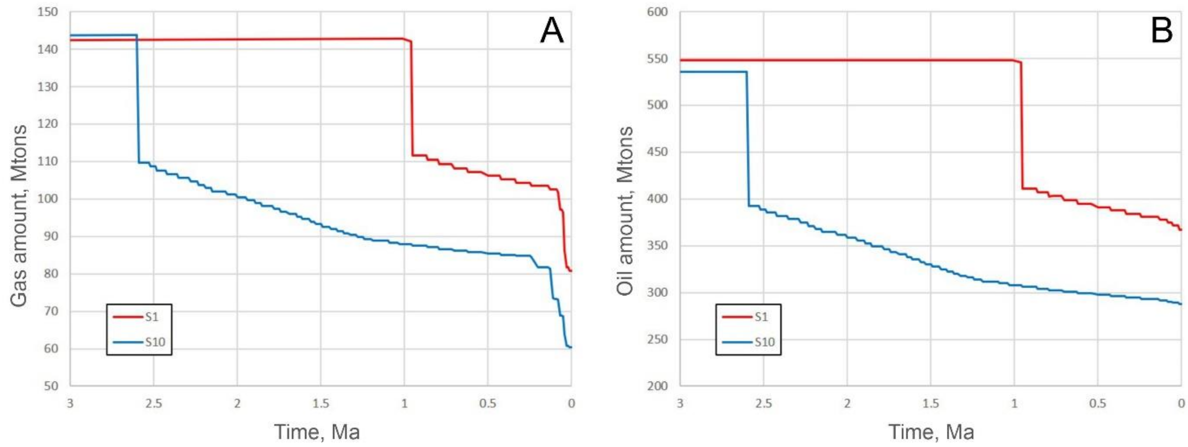

Figure 10. Graphs of gas (A) and oil (B) amount in Realgrunnen from 3 till 0 Ma (S1,10 – Scenarios 1, 10)

4.2. Comparison of models for two sections (Scenario 7)

Section NBR06RE11-148600 exhibits a significant structural high with an eroded top (Figures 2, 11), which makes it principally different from the NBR07-249214 section. For evaluating the influence of this difference on the fluid leakage, we test the NBR06 model in Scenario 7, where only leakage due to the seal breach is considered and faults are neglected. Erosion of the potential anticlinal trap in the NBR06 model should directly impact accumulation and leakage since the reservoir lacks the seal. Reconstruction of the geometry of the anticlinal stratigraphic horizons before the erosion (Figure 11b) indicates that the maximum distance between URU and the proposed top of the anticline is ca. 70 m.

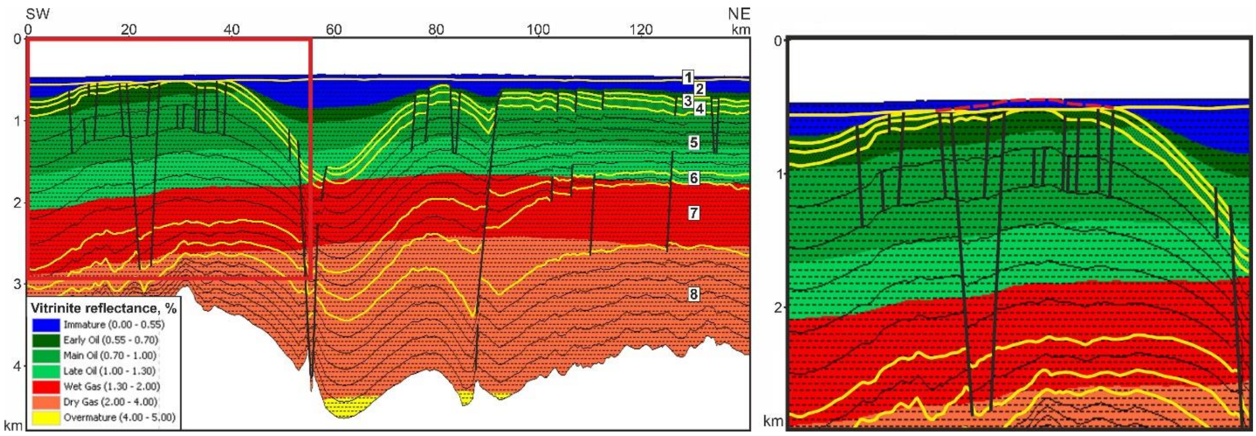

(a) (b)

Figure 11. Simulated section exhibiting present-day thermal maturation by values of vitrinite reflectance for the NBR06 model (a) with a scaled-up fragment of the eroded anticline (b). Layers in the section: 1 – Nordland Group, 2 – Kolmule-Knurr formations, 3 – Hekkingen-Fuglen formations, 4 – Realgrunnen Subgroup, 5 – Snadd Formation, 6 – Kobbe Formation, 7 – Klappmys Formation, 8 – Havert Formation. Red dashed line – restored top of the anticline before erosion

Glacial erosion is equally distributed between all cycles. At the location of the demonstrated anticline, approximate net erosion for each glacial cycle is ca. 75 m based on the erosion map by Henriksen et al. (2011a) equally divided by the number of assumed glacial cycles. Therefore, we propose that erosion of the anticlinal trap is confined to the last glacial cycle, as the height of the eroded top part of the anticline is slightly smaller than the total proposed thickness of deposits eroded during a single glacial cycle. However, our results reveal intensive gas leakage occurring already from 0.05 Ma after the critical thickness of rocks overlying the reservoir is reached, before the last glacial cycle (Figure 12). Hence, erosion of the anticlinal trap appears not to have contributed significantly to the total gas leakage. Erosion of the trap would have initiated intensive gas leakage if it had happened before the thickness of rocks overlying the Realgrunnen reservoir reached the critically small value for the seal breach. However, this does not seem to be the case in our study area.

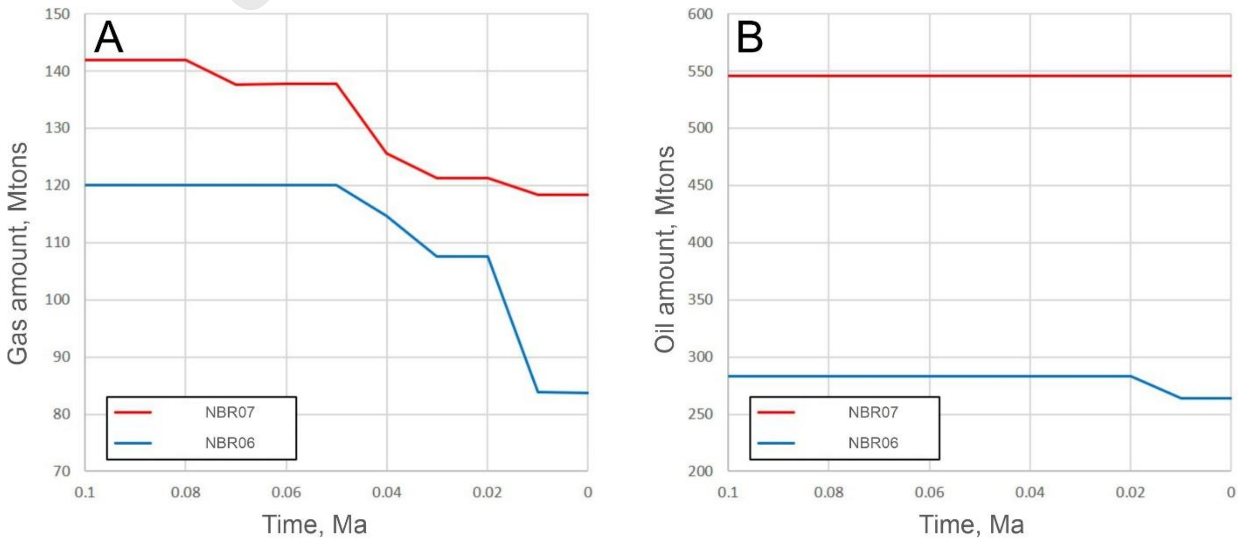

Figure 12. Graph of gas (A) and oil (B) amount in Realgrunnen from 0.1 till 0 Ma for the NBR07 and NBR06 models (Scenario 7)

Gas leakage due to seal breach in the NBR06 model happens later, in comparison with the NBR07 model section, due to the smaller amount of gas pressurizing the seal (Figure 12A). Oil in the NBR06 model leaks only at the period related to the last glaciation, in which the seal is assigned to become eroded (Figure 12B). This is consistent with the NBR07 model where oil does not leak through the existing seal, provided that faults are not conductive.

5. Discussion

5.1.Effects of gas leakage on oil preservation

The common feature for different scenarios of modeling was the clear difference in migration ability of oil and gas. Gas can leak from the reservoir as a result of the seal breach after reaching critically small overburden pressure, while oil escapes the reservoir only through conductive faults. This result is consistent with known patterns of oil and gas behavior in response to erosion (e.g., Sales, 1997; Karlsen, Skeie, 2006; Ohm et al., 2008).

In general, erosion and uplift of an area cause pressure decrease in the sedimentary cover, which can lead to redistribution of accumulated hydrocarbons. If an anticline trap is filled with hydrocarbons to spill points, expanding gas can force oil in accumulations to leak out of spill and migrate laterally to shallower structures (e.g., Nyland et al., 1992; Henriksen et al., 2011b; Lerch et al., 2016, Tasianas et al., 2016). However, gas trapped in an anticline is highly susceptible to upward leakage in the case of seal disintegration due to faulting, fracturing or capillary leakage (e.g., Ohm et al., 2008; Dore et al., 2002). Therefore, in a particular accumulation, gas volume is increasing during uplift due to exsolution of lighter hydrocarbons out of the petroleum phase, as long as the seal is capable of trapping it. If gas escapes from the trap, the latter might consequently retain mainly oil, which is less mobile than gas (Sales, 1997; Karlsen, Skeie, 2006). Such a mechanism of gas bleed off has been proposed for the Goliat Field in the Hammerfest Basin (Ohm et al., 2008).

The Hanssen and Wisting discoveries located in our study area are reported to contain mainly oil (NPD FactPages). We propose that large gas volumes could have been present in the reservoirs of these discoveries and further leaked upwards through faults, seal breach and, possibly, fractures in the seal. If gas leakage had not been intensive enough, gas expansion during successive erosion and uplift could have forced oil out of the traps over spill points. Thus, intensive gas leakage could have been the key circumstance for oil preservation in the Hanssen and Wisting discoveries. Initially, oil, apart from that generated in vicinity of the Hanssen and Wisting structures, could have migrated to the discoveries laterally, from structures with reservoirs of the same stratigraphic level, but located deeper. The supporting fact for this hypothesis is the existence of a large gas discovery of Intrepid Eagle in the central Bjørnøyrenna (Figure 1), where the Stø (Realgrunnen) reservoir is deeper than in the Hanssen and Wisting structures (Top at 846 m below sea level, opposed to 672 m and 635 m respectively; NPD FactPages). Oil might have been present there in the past, and further, due to gas expansion, escaped within the reservoir to shallower traps where due to seal failure, gaseous hydrocarbons could have leaked upwards, thus preserving oil masses.

5.2. Feasibility of the seal breach

During burial, potential sealing rocks in a sedimentary basin undergo compaction and their capillary pressure gradually increases, which improves their sealing properties. However, the opposite situation is typical for uplift and erosion (Jin et al., 2014; Yuan et al., 2011). Apart from seal capillary pressure decrease, another trigger for hydrocarbon leakage is fracturing of the seal. In soil mechanics, there is a special term for a material which experiences effective overburden pressures lower than the maximum in the past – it is called overconsolidated, as opposed to a normally consolidated material that is subjected to its maximum experienced effective overburden pressure (Das, 2008). When studying these materials, the overconsolidation ratio (OCR) is commonly used:

$$\mathrm{OCR} = \frac{\sigma'_c}{\sigma'_o}, \tag{1}$$

Where σ'_o is the present effective overburden pressure and σ'_c is the maximum value of this parameter in geological history.

Nygård et al. (2006) conducted experimental studies of mechanical features of the Upper Jurassic Kimmeridge clays, found onshore UK, in response to their sealing qualities. They showed that normally consolidated rocks are characterized by ductile features, whereas overconsolidated ones are more brittle. They also proposed that leakage of hydrocarbons through sealing shales happens when the OCR ratio of the latter exceeds the threshold value of 2.5, as a result of formation of fractures.

In our study, the Hekkingen-Fuglen seal consists of overconsolidated shales, which are age analogues of the rocks studied by Nygård et al. (2006). We calculate approximate values of OCR for the base of the seal at the location of the Hanssen Discovery, for the time corresponding to the modelled seal breach, assuming that effective overburden pressure is hydrostatic. Maximum overburden pressure should have occurred either at the time of the deepest burial of the sedimentary cover before the regional uplift or at the onset of glaciations during the Quaternary.

The net thickness of eroded deposits at the Hanssen Discovery location is ca. 2200 m (Henriksen et al., 2011a). Following our main scenario, at the time of the seal breach, its base (the reservoir top) is at a depth of ca. 290 m below the seafloor, experiencing a total hydrostatic pressure of ca. 9.1 MPa, as stated earlier. For the maximum burial time we assume no water column, as it is the beginning of erosion. By adding the thickness of eroded deposits and excluding the glacial Nordland sequence (48 m) from the present-day Fuglen base depth below seafloor (254 m), two latter values being documented for the well 7324/7-2 (NPD FactPages), we find that the Realgrunnen reservoir is assumed to have been buried by sedimentary volume with the maximum thickness of ca. 2406 m (254 m – 48 m + 2200 m), experiencing maximum overburden hydrostatic pressure of ca. 24.1 MPa. Therefore, the OCR ratio at the time of the seal breach equals ca. 2.6 (24.1 MPa / 9.1 MPa).

We consider that maximum overburden pressure due to an ice sheet occurred during the first glacial cycle, assuming the same ice sheet thicknesses for all cycles prior to Early Weichselian, equal to that of the latter stage (ca. 2000 m, according to the UiT-ISM model). Assuming that half of the total erosion is preglacial, maximum overburden thickness for the time of the first glaciation is ca. 3306 (254 m – 48 m + 2200 m / 2 + 2000 m) corresponding to pressure of ca. 33.1 MPa which is higher than that calculated for the maximum burial time. In this case, OCR ratio at the time of the seal breach equals ca. 3.6 (33.1 MPa / 9.1 MPa).

Nevertheless, basin modeling conducted in this study does not account for the effect of fracturing of the overconsolidated seals described above. The gas leakage revealed in the modeling, not connected with faults, is caused by excess gas pressure in the reservoir over capillary entry pressure of the seal. However, the fact that by the time of leakage through the seal the OCR ratio of the seal exceeds the threshold value (2.5), defined by experimental studies (Nygård et al., 2006), we can hypothesize that apart from capillary leakage modeled in our research, additional leakage could have happened due to possible fracturing of the overconsolidated seal. Thus, real amount of hydrocarbon leakage might be higher than what is shown in our modeling.

5.3. Comparison with other studies

We compare results of our research with other basin and petroleum system modeling studies from the Barents Sea. The study of the Hammerfest Basin by Ostanin et al. (2017) suggests somewhat similar trends of hydrocarbon leakage. Ostanin et al. (2017) propose several scenarios with different values of permeabilities of faults, from closed to highly conductive. Similar to this study, leakage was modeled to happen abruptly through faults during the first deglaciation, then slightly reducing during subsequent deglaciations. The main difference from the results of our research is that there is no observed abrupt leakage due to breach of the seal. Basin modeling, conducted for the Hammerfest Basin by Duran et al. (2013), does not consider faults, and abrupt leakage due to seal breach is not observed. However, certain amounts of capillary leakage are recognized during periods of ice retreat and interglacials.

The reason why a breach of the seal is not predicted in the Hammerfest Basin may be explained by differences in the depth of the reservoir and seal units. The Stø (Realgrunnen) reservoir is currently much deeper than in the study area of the Bjarmeland Platform. According to the NPD Factpages, on the Snøhvit Field, in the well 7121/4-1 (as an example), the top of the Stø Formation is at a depth of 1961 m below the seafloor, with an additional 335 m of water column. This corresponds to hydrostatic pressure of ca. 23 MPa. These depths and pressures were much higher before the erosion. The critical pressure from overlying rocks for seal breach obtained in this study is significantly less than what is currently present at the Stø Formation on the Snøhvit Field of the Hammerfest Basin. Henriksen et al. (2011a) show total thicknesses of eroded deposits for the Hammerfest Basin from 800 to 1600 m. Adding the highest thickness of eroded deposits to the well 7121/4-1 and excluding glacial Nordland sequence, the maximum overburden thickness for the top of the Stø Formation at the deepest burial time equals 3471 m (1961 m – 90 m + 1600 m), present-day OCR being equal to ca. 1.5 (34.71 MPa / 23 MPa). The maximum ice sheet thickness for the Hammerfest Basin is approximately 1620 m (according to the UiT-ISM model). Assuming that half of total erosion is preglacial, maximum overburden thickness for the time of the first glaciation is ca. 4291 (1961 m – 90 m + 1600 m / 2 + 1620 m) and corresponding OCR is ca. 1.9 (42.91 MPa / 23 MPa). Obtained OCR values for the well on the Snøhvit Field are lower than the abovementioned threshold (2.5), which might provide additional constraint for leakage through the seal in the Hammerfest Basin.

5.4. Analysis of seismic features of possible leakage

To support our modeling results with empirical data, we explore available 3D seismic surveys covering our study area for possible evidence of hydrocarbon migration. Available data demonstrates features indicating probable gas migration from the Realgrunnen reservoir. Here we document two examples of relevant seismic sections. The first example is from a conventional seismic survey corresponding to the area within the Bjarmeland Platform (Figure 13). The seal layer, composed of the Hekkingen and Fuglen formations, is intensively displaced by faults. Above Top Hekkingen, around the upper continuations of the faults, chaotic seismic reflections are distinguished, which may indicate gas leakage through the faults from the Realgrunnen Reservoir. Leakage might also occur from lower layers as several bright spots can be identified adjacent to a major fault plane extending to great depth. These observations are similar to what Vadakkepuliyambatta et al. (2013) observed in the SW Barents Sea.

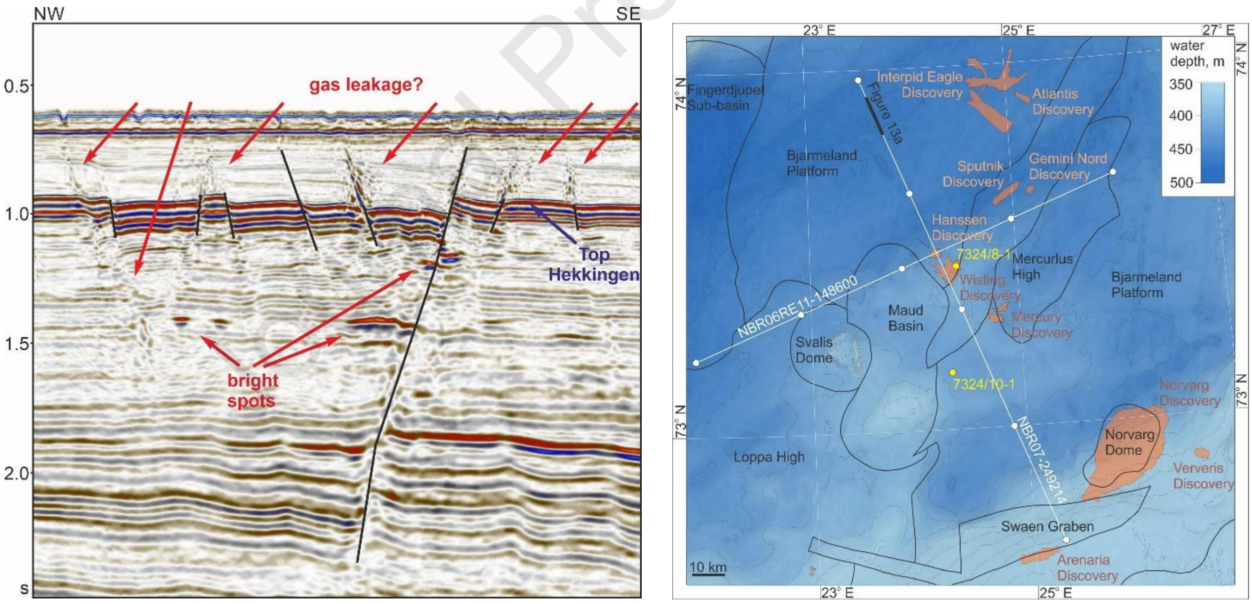

(a) **(b)**

Figure 13. a) Fragment of a section from the seismic cube HOOP_PRCMIG for the line assigned along the NBR07-249214 seismic line. Seismic data courtesy of TGS. **b)** Location of the fragment (black line in the map).

The second example is from the high-resolution seismic survey TGS16004 (Figure 14). The anticline in the section corresponds to the Hanssen Field. A bright spot is visible, indicating a possible gas cap, as well as two flat spots. Considering the fact that Hanssen is reported to be an oil discovery (NPD Factpages), the two flat spots might mark the upper and lower limits of an oil column. The upper one, which is brighter, might refer to a gas-oil contact, the lower one – to an oil-water contact. Between Top Hekkingen and URU, some bright seismic reflections are clearly visible. These features might indicate possible gas leakage from the reservoir through the seal, as faults are not abundant below these features. However, we do not consider these reflections as a definite support of the leakage due to the seal breach, as they might also be associated with other geological features.

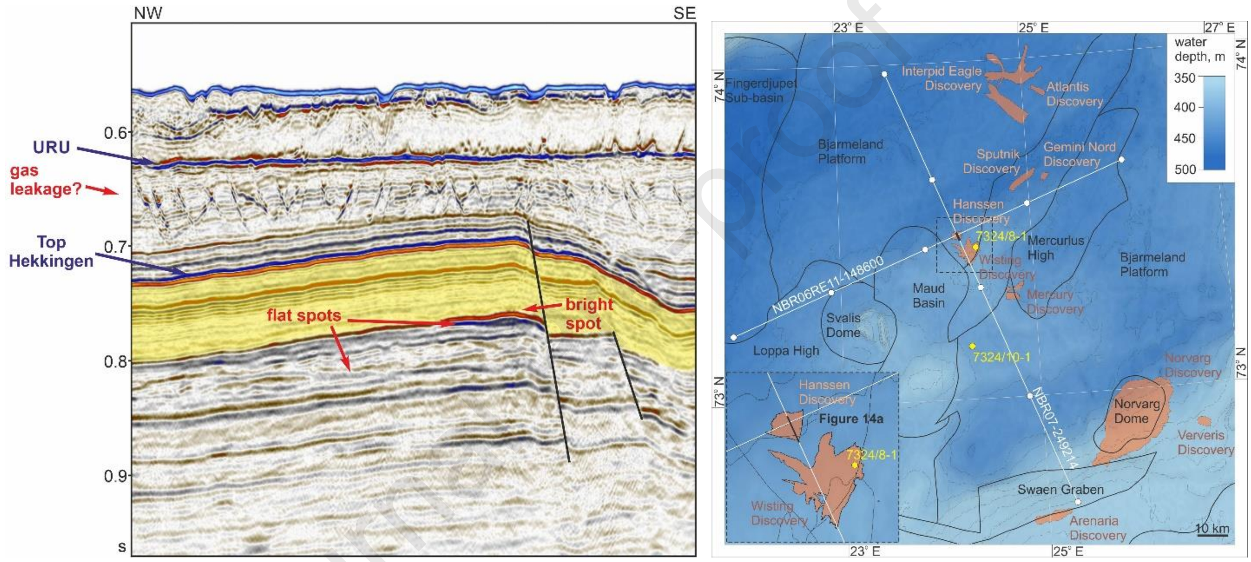

(a) (b)

Figure 14. a) Fragment of a section from the seismic cube TGS16004 for the line assigned along the NBR07-249214 seismic line. Seismic data courtesy of TGS. Yellow-shaded zone – seal layer (Hekkingen and Fuglen formations). **b)** Location of the fragment (black line in the map).

5.5. Possible connection with gas hydrates and gas release through the seabed

Hydrocarbons leaking from the Realgrunnen reservoir within Bjørnøyrenna could either accumulate in permeable zones of the shallow subsurface or escape through the seabed. Seabed methane release could also be modulated by gas hydrates forming beneath grounded ice sheets and likely acting as a dynamic capacitor for gas migrating from petroleum systems (Portnov et al., 2016; Serov et al., 2017; Andreassen et al., 2017). During episodes of grounded ice retreat, ice mass loss caused depressurization of the underlying strata leading to gas hydrate dissociation. Due to the capacitor effect of the gas hydrates and slow isostatic readjustment of the crust after deglaciation (Andreassen et al. 2017), the seabed release of methane gas from the petroleum systems might be delayed. Thus, the seabed leakage may not be simultaneous with gas migration from the petroleum systems. Moreover, today, significant parts of Bjørnøyrenna lie within the methane hydrate stability zone (e.g., Vadakkepuliyambatta et al., 2017; Bogoyavlensky et al., 2018), which also could have been the case during interglacials earlier in Quaternary if the water depths and the near-bottom temperatures were favorable (Chand et al., 2012; Andreassen et al., 2017).

The existence of free gas, either microbial or thermogenic, under gas hydrates generally increases the probability of seafloor blowouts, particularly for areas where the gas hydrate stability zone is thinning due to warming and/or depressurization (Andreassen et al., 2017). For areas with no gas hydrates or other seal rocks in the shallow subsurface, gradual seepage is a more likely mechanism of gas release. However, regardless of the release process, the question regarding the origin of gas in the shallow subsurface remains speculative. For instance, in the nearby cluster of craters (Figure 1), thermogenic hydrate-forming gas is thought to have migrated from deeper reservoirs through faults (Andreassen et al., 2017; Waage et al., 2020).

Our current research contributes to solving the question of gas migration, as we demonstrate that the seal breach in underlying hydrocarbon plays could have modulated vertical gas migration into the shallow subsurface. Leakage due to seal breach seems to be significant for anticlinal structures located in zones of remarkably intensive erosion and uplift. Such settings are expected in most areas of Bjørnøyrenna, however, not excluding other parts of the Barents Sea that were intensively eroded in the Cenozoic. Leakage through faults remains an effective mechanism for hydrocarbon migration, which might be widespread within the Barents Sea region and is not directly dependent on the erosional history.

6. Conclusions

By utilizing 2D basin and petroleum system modeling forced by a quantitatively constrained glacial history, we provide insights into the patterns and timing of hydrocarbon leakage from shallow reservoirs in the south-western Barents Sea during the Quaternary. Most intense fault-driven leakage occurred during the first deglaciation which is proposed to have been during the period of 0.96-0.95 Ma, with relatively smaller leakage occurring during subsequent glacial cycles. Significant leakage of gas additionally occurs by the seal breach once glacial erosion reduces the overburden pressure from rocks overlying the reservoir to a critical hydrostatic pressure of ca. 9.1 MPa (up to 10.4 MPa, depending on the hydrocarbon saturation of the reservoir). We estimate that up to ca. 20% of accumulated gas and oil leaked during the first glacial cycle through the open faults and up to ca. 15 % of the initial amount of gas escaped after the seal breach. However, sensitivity analyses indicate seal breach can cause up to 26 % of gas loss. Total leakage during the whole period of glaciations is estimated at ca. 40 % of gas accumulated by the first glacial cycle and ca. 30 % of oil, with sensitivity tests giving maximum values of 58 % and 46 % respectively.

Sensitivity experiments allow us to conclude that uncertainties in parameters of heat flow, geochemistry (TOC), and the thickness of ice sheets do not significantly influence the timing and extent of leakage events. The most important factors affecting gas leakage are total net erosion and the ratio between glacial and preglacial erosion, as these directly impact the volumes of accumulated hydrocarbons. Different gas saturations of the reservoir result in different reservoir pressures, and thus shift the value of the critical overburden thickness that controls the initiation of gas leakage. The glacial history (number and timing of glaciations) is also important in terms of the timing of when critical overburden pressure for gas leakage through the seal is reached.

Comparison of the basin and petroleum system modeling results with earlier experimental studies of overconsolidated rocks suggests that additional leakage through the seal might happen due to fracturing of seal rocks as they become brittle after burial and further uplift. Seismic data from the study area exhibit features indicative of gas leakage, supporting the results of the conducted basin and petroleum system modeling.

Acknowledgements

We are thankful to TGS for providing some of the seismic data. We also thank the Norwegian Petroleum Directorate (NPD) for access to the Norwegian repository for petroleum data. We are grateful to Schlumberger for providing Petrel and PetroMod software packages and support. We express gratitude to Rüdiger Lutz from the Federal Institute for Geosciences and Natural Resources (BGR), and to an anonymous reviewer for their useful comments at the revision stage which helped to improve the article.

This work was supported by the Research Council of Norway (RCN) through its Centres of Excellence funding scheme, project no. 223259.

References

Abay, T. B., Karlsen, D. A., Pedersen, J. H., Olaussen, S., & Backer-Owe, K. (2018). Thermal maturity, hydrocarbon potential and kerogen type of some Triassic–Lower Cretaceous sediments from the SW Barents Sea and Svalbard. Petroleum Geoscience, 24(3), 349-373. DOI: https://doi.org/10.1144/petgeo2017-035

Al-Hajeri, M. M., Al Saeed, M., Derks, J., Fuchs, T., Hantschel, T., Kauerauf, A., Neumaier, M., Schenk, O., Swientek, O., Tessen, N., Welte, D., Wygrala, B., Kornpihl, D., & Peters K (2009). Basin and petroleum system modeling. Oilfield Review, 21(2), 14-29.

Andreassen, K., Hubbard, A., Winsborrow, M., Patton, H., Vadakkepuliyambatta, S., Plaza-Faverola, A., Gudlaugsson, E., Serov, P., Deryabin, A., Mattingsdal, R., Mienert, J., & Bünz S. (2017). Massive blow-out craters formed by hydrate-controlled methane expulsion from the Arctic seafloor. Science, 356(6341), 948-953. DOI: 10.1126/science.aal4500

Berglund, L. T., Augustson, J., Færseth, R., Gjelberg, J., & Ramberg-Moe, H. (1986). The evolution of the Hammerfest Basin. In Habitat of hydrocarbons on the Norwegian continental shelf. International conference (pp. 319-338).

Bogoyavlensky, V., Bogoyavlensky, I., Nikonov, R., & Kishankov, A. (2020). Complex of Geophysical Studies of the Seyakha Catastrophic Gas Blowout Crater on the Yamal Peninsula, Russian Arctic. Geosciences, 10(6), 215. DOI: https://doi.org/10.3390/geosciences10060215

Bogoyavlensky, V., Kishankov, A., Yanchevskaya, A., & Bogoyavlensky, I. (2018). Forecast of gas hydrates distribution zones in the Arctic Ocean and adjacent offshore areas. Geosciences, 8(12), 453. DOI: https://doi.org/10.3390/geosciences8120453

Bogoyavlensky, V. I., Sizov, O. S., Bogoyavlensky, I. V., Nikonov, R. A., Kishankov, A. V., & Kargina, T. N. (2019, September). Study of the Seyakha Gas Explosion on the Yamal Peninsula. In Geomodel 2019 (Vol. 2019, No. 1, pp. 1-5). European Association of Geoscientists & Engineers. DOI: https://doi.org/10.3997/2214-4609.201950125

Boyer, T.P., Baranova, O.K., Coleman, C., Garcia, H.E., Grodsky, A., Locarnini, R.A., Mishonov, A.V., Paver, C.R., Reagan, J.R., Seidov, D., Smolyar, I.V., Weathers, K., Zweng, M.M. (2018). World Ocean Database 2018. A.V. Mishonov, Technical Ed., NOAA Atlas NESDIS 87.

Cartwright, J., Huuse, M., & Aplin, A. (2007). Seal bypass systems. AAPG bulletin, 91(8), 1141-1166. DOI: https://doi.org/10.1306/04090705181

Chand, S., Thorsnes, T., Rise, L., Brunstad, H., Stoddart, D., Bøe, R., Lågstad, P., & Svolsbru, T. (2012). Multiple episodes of fluid flow in the SW Barents Sea (Loppa High) evidenced by gas flares, pockmarks and gas hydrate accumulation. Earth and Planetary Science Letters, 331, 305-314. DOI: https://doi.org/10.1016/j.epsl.2012.03.021

Chapman, R. E. (1983). Petroleum geology. Elsevier.

Cunningham, R., & Lindholm, R. M. (2000). AAPG Memoir 73, Chapter 8: Seismic Evidence for Widespread Gas Hydrate Formation, Offshore West Africa.

Dalland, A., Worsley, D. & Ofstad, K. (eds), 1988. A lithostratigraphical scheme for the Mesozoic and Cenozoic succession offshore Mid- and Northern Norway. Norwegian Petroleum Directorate Bulletin, 4, 1 - 65.

Das, B. M. (2008). Advanced Soil mechanics. Tylor & Frances.

Dengo, C. A., & Røssland, K. G. (1992). Extensional tectonic history of the western Barents Sea. In Structural and tectonic modelling and its application to petroleum geology (pp. 91-107). Elsevier. DOI: https://doi.org/10.1016/B978-0-444-88607-1.50011-5

Dimakis, P., Braathen, B. I., Faleide, J. I., Elverhøi, A., & Gudlaugsson, S. T. (1998). Cenozoic erosion and the preglacial uplift of the Svalbard–Barents Sea region. Tectonophysics, 300(1-4), 311-327. DOI: https://doi.org/10.1016/S0040-1951(98)00245-5

Doré, A. G. (1995). Barents Sea geology, petroleum resources and commercial potential. Arctic, 207-221.

Doré, A. G., Scotchman, I. C., & Corcoran, D. (2000). Cenozoic exhumation and prediction of the hydrocarbon system on the NW European margin. Journal of Geochemical Exploration, 69, 615-618. DOI: https://doi.org/10.1016/S0375-6742(00)00137-0

Doré, A. G., Cartwright, J. A., Stoker, M. S., Turner, J. P., & White, N. J. (Eds.). (2002). Exhumation of the North Atlantic margin: timing, mechanisms and implications for petroleum exploration. Geological Society of London.

Downey, M. W. (1984). Evaluating seals for hydrocarbon accumulations. AAPG bulletin, 68(11), 1752-1763. DOI: https://doi.org/10.1306/AD461994-16F7-11D7-8645000102C1865D

Duran, E. R., di Primio, R., Anka, Z., Stoddart, D., & Horsfield, B. (2013). 3D-basin modelling of the Hammerfest Basin (southwestern Barents Sea): A quantitative assessment of petroleum generation, migration and leakage. Marine and petroleum geology, 45, 281-303. DOI: https://doi.org/10.1016/j.marpetgeo.2013.04.023

Fabel, D., Stroeven, A. P., Harbor, J., Kleman, J., Elmore, D., & Fink, D. (2002). Landscape preservation under Fennoscandian ice sheets determined from in situ produced 10Be and 26Al. Earth and Planetary Science Letters, 201(2), 397-406. DOI: https://doi.org/10.1016/S0012-821X(02)00714-8

Norwegian Petroleum Directorate. FactPages. Available online: https://factpages.npd.no/en (Accessed on 20th October 2021)

Faleide, J. I., Solheim, A., Fiedler, A., Hjelstuen, B. O., Andersen, E. S., & Vanneste, K. (1996). Late Cenozoic evolution of the western Barents Sea-Svalbard continental margin. Global and Planetary Change, 12(1-4), 53-74. DOI: https://doi.org/10.1016/0921-8181(95)00012-7

Faleide, J. I., Tsikalas, F., Breivik, A. J., Mjelde, R., Ritzmann, O., Engen, O., Wilson, J., & Eldholm, O. (2008). Structure and evolution of the continental margin off Norway and the Barents Sea. Episodes, 31(1), 82-91.

Faleide, J. I., Bjørlykke, K., & Gabrielsen, R. H. (2015). Geology of the Norwegian continental shelf. In Petroleum Geoscience (pp. 603-637). Springer, Berlin, Heidelberg.

Freire, A. F. M., Matsumoto, R., & Santos, L. A. (2011). Structural-stratigraphic control on the Umitaka Spur gas hydrates of Joetsu Basin in the eastern margin of Japan Sea. Marine and Petroleum Geology, 28(10), 1967-1978. DOI: https://doi.org/10.1016/j.marpetgeo.2010.10.004

Gabrielsen, R. H., Faerseth, R. B., & Jensen, L. N. (1990). Structural elements of the Norwegian continental shelf. Pt. 1. The Barents Sea region. Norwegian Petroleum Directorate.

Gac, S., Hansford, P. A., & Faleide, J. I. (2018). Basin modelling of the SW Barents Sea. Marine and Petroleum Geology, 95, 167-187. DOI: https://doi.org/10.1016/j.marpetgeo.2018.04.022

Geological assessment of petroleum resources in eastern parts of Barents Sea North (2017). Norwegian Petroleum Directorate.

Glørstad-Clark, E., Faleide, J. I., Lundschien, B. A., & Nystuen, J. P. (2010). Triassic seismic sequence stratigraphy and paleogeography of the western Barents Sea area. Marine and Petroleum Geology, 27(7), 1448-1475. DOI: https://doi.org/10.1016/j.marpetgeo.2010.02.008

Glørstad-Clark, E., Birkeland, E. P., Nystuen, J. P., Faleide, J. I., & Midtkandal, I. (2011). Triassic platform-margin deltas in the western Barents Sea. Marine and Petroleum Geology, 28(7), 1294-1314. DOI: https://doi.org/10.1016/j.marpetgeo.2011.03.006

Gramberg, I. S., Suprunenko, O. I., & Lazurkin, D. V. (2000). Petroleum potential of the Arctic Ocean. Geological Structure and Geomorphology of the Arctic in View of the Problem of the Outer Limit of the Continental Shelf of the Russian Federation in the Arctic Waters [in Russian]. VNIIOkeangeologiya, 31-38.

Grunau, H. R. (1987). A worldwide look at the cap- rock problem. Journal of Petroleum Geology, 10(3), 245-265.

Henriksen, E., Bjørnseth, H. M., Hals, T. K., Heide, T., Kiryukhina, T., Kløvjan, O. S., Larssen, G. B., Ryseth, A. E., Rønning, K., Sollid, K., & Stoupakova, A. (2011a). Uplift and erosion of the greater Barents Sea: impact on prospectivity and petroleum systems. Geological Society, London, Memoirs, 35(1), 271-281. DOI: https://doi.org/10.1144/M35.17

Henriksen, E., Ryseth, A. E., Larssen, G. B., Heide, T., Rønning, K., Sollid, K., & Stoupakova, A. V. (2011b). Tectonostratigraphy of the greater Barents Sea: implications for petroleum systems. Geological Society, London, Memoirs, 35(1), 163-195. DOI: https://doi.org/10.1144/M35.10

Jin, Z., Yuan, Y., Sun, D., Liu, Q., & Li, S. (2014). Models for dynamic evaluation of mudstone/shale cap rocks and their applications in the Lower Paleozoic sequences, Sichuan Basin, SW China. Marine and petroleum geology, 49, 121-128. DOI: https://doi.org/10.1016/j.marpetgeo.2013.10.001

Judd, A., & Hovland, M. (2007). Seabed Fluid Flow: The Impact on Geology. Biology and the Marine Environment. Cambridge.

Karlsen, D. A., & Skeie, J. E. (2006). Petroleum migration, faults and overpressure, part I: calibrating basin modelling using petroleum in traps—a review. Journal of Petroleum Geology, 29(3), 227-256.

Kvenvolden, K. A. (1988). Methane hydrate—a major reservoir of carbon in the shallow geosphere? Chemical geology, 71(1-3), 41-51. DOI: https://doi.org/10.1016/0009-2541(88)90104-0

Lasabuda, A. P., Johansen, N. S., Laberg, J. S., Faleide, J. I., Senger, K., Rydningen, T. A., Patton, H., Knutsen, S.-M., & Hanssen, A. (2021). Cenozoic uplift and erosion on the Norwegian Barents Shelf–A review. Earth-Science Reviews, 103609. DOI: https://doi.org/10.1016/j.earscirev.2021.103609

Lerch, B., Karlsen, D. A., Abay, T. B., Duggan, D., Seland, R., & Backer-Owe, K. (2016). Regional petroleum alteration trends in Barents Sea oils and condensates as a clue to migration regimes and processes. AAPG Bulletin, 100(2), 165-190. DOI: https://doi.org/10.1306/08101514152

Lisiecki, L. E., & Raymo, M. E. (2005). A Pliocene- Pleistocene stack of 57 globally distributed benthic δ18O records. Paleoceanography, 20(1). DOI:10.1029/2004PA001071

Lundschien, B. A., Høy, T., & Mørk, A. (2014). Triassic hydrocarbon potential in the Northern Barents Sea; integrating Svalbard and stratigraphic core data. Norwegian Petroleum Directorate Bulletin, 11(11), 3-20.

Max, M. D., & Lowrie, A. (1993). Natural gas hydrates: Arctic and Nordic Sea potential. In Norwegian Petroleum Society Special Publications (Vol. 2, pp. 27-53). Elsevier. https://doi.org/10.1016/B978-0-444-88943-0.50007-1

Mørk, A., Dallmann, W.K., Dypvik, H., Johannessen, E.P., Larssen, G.B., Nagy, J., Nøttvedt, A., Olaussen, S., Pcelina, T.M., & Worsley, D. (1999). Mesozoic Lithostratigraphy. In: Dallmann W.K. (ed.), Lithostratigraphic Lexicon of Svalbard: Upper Paleozoic to Quaternary Bedrock. Review and Recommendation for Nomenclature Use. Norwegian Polar Institute, Tromsø, 127 – 214.

Nygård, R., Gutierrez, M., Bratli, R. K., & Høeg, K. (2006). Brittle–ductile transition, shear failure and leakage in shales and mudrocks. Marine and Petroleum Geology, 23(2), 201-212. DOI: https://doi.org/10.1016/j.marpetgeo.2005.10.001

Nyland, B., Jensen, L. N., Skagen, J. L., Skarpnes, O., & Vorren, T. (1992). Tertiary uplift and erosion in the Barents Sea: magnitude, timing and consequences. In Structural and tectonic modelling and its application to petroleum geology (pp. 153-162). Elsevier. DOI: https://doi.org/10.1016/B978-0-444-88607-1.50015-2

Nøttvedt, A., Berglund, L. T., Rasmussen, E., & Steel, R. J. (1988). Some aspects of Tertiary tectonics and sedimentation along the western Barents Shelf. Geological Society, London, Special Publications, 39(1), 421-425. DOI: https://doi.org/10.1144/GSL.SP.1988.039.01.37

Nøttvedt, A., Cecchi, M., Gjelberg, J. G., Kristensen, S. E., Lønøy, A., Rasmussen, A., Rasmussen, E., Skott, P.H., & Van Veen, P. M. (1993). Svalbard-Barents Sea correlation: a short review. In Norwegian Petroleum Society Special Publications (Vol. 2, pp. 363-375). Elsevier. DOI: https://doi.org/10.1016/B978-0-444-88943-0.50027-7

Ohm, S. E., Karlsen, D. A., & Austin, T. J. F. (2008). Geochemically driven exploration models in uplifted areas: Examples from the Norwegian Barents Sea. AAPG bulletin, 92(9), 1191-1223. DOI: https://doi.org/10.1306/06180808028

Ostanin, I., Anka, Z., & Di Primio, R. (2017). Role of faults in hydrocarbon leakage in the Hammerfest Basin, SW Barents Sea: Insights from seismic data and numerical modelling. Geosciences, 7(2), 28. DOI: https://doi.org/10.3390/geosciences7020028

Pascal, C., Balling, N., Barrere, C., Davidsen, B., Ebbing, J., Elvebakk, H., Mesli, M., Roberts, D., Slagstad, T., & Willemoes-Wissing, B. (2010). HeatBar final report 2010. Basement heat generation and heat flow in the western Barents Sea – Importance for hydrocarbon systems. NGU Report, 30.

Patton, H., Hubbard, A., Andreassen, K., Auriac, A., Whitehouse, P. L., Stroeven, A. P., Shackleton, C., Winsborrow, M., Heyman, J., & Hall, A. M. (2017). Deglaciation of the Eurasian ice sheet complex. Quaternary Science Reviews, 169, 148-172. DOI: https://doi.org/10.1016/j.quascirev.2017.05.019

Patton, H., Hubbard, A., Andreassen, K., Winsborrow, M., & Stroeven, A. P. (2016). The build-up, configuration, and dynamical sensitivity of the Eurasian ice-sheet complex to Late Weichselian climatic and oceanic forcing. Quaternary Science Reviews, 153, 97-121. DOI: https://doi.org/10.1016/j.quascirev.2016.10.009

Paull, C. K., Normark, W. R., Ussler III, W., Caress, D. W., & Keaten, R. (2008). Association among active seafloor deformation, mound formation, and gas hydrate growth and accumulation within the seafloor of the Santa Monica Basin, offshore California. Marine Geology, 250(3-4), 258-275. DOI: https://doi.org/10.1016/j.margeo.2008.01.011

Pepper, A. S., & Corvi, P. J. (1995). Simple kinetic models of petroleum formation. Part I: oil and gas generation from kerogen. Marine and petroleum geology, 12(3), 291-319. DOI: https://doi.org/10.1016/0264-8172(95)98381-E

Peters, K.E., Curry, D.J., Kacewicz, M. (2012). An overview of basin and petroleum system modeling; definitions and concepts. In: Peters, K.E., Curry, D.J., Kacewicz, M. (Eds.), Basin Modeling: New Horizons in Research and Applications. AAPG Hedberg Series 4, Tulsa, OK, United States, 1-17. DOI:10.1306/13311426H4139

Portnov, A., Vadakkepuliyambatta, S., Mienert, J., & Hubbard, A. (2016). Ice-sheet-driven methane storage and release in the Arctic. Nature communications, 7(1), 1-7.

Reemst, P., Cloetingh, S., & Fanavoll, S. (1994). Tectonostratigraphic modelling of Cenozoic uplift and erosion in the south-western Barents Sea. Marine and Petroleum Geology, 11(4), 478-490. DOI: https://doi.org/10.1016/0264-8172(94)90081-7

Rise, L., Bellec, V. K., Chand, S., & Bøe, R. (2014). Pockmarks in the southwestern Barents Sea and Finnmark fjords. Norwegian Journal of Geology/Norsk Geologisk Forening, 94(4).

Roberts, D., & Gee, D. G. (1985). An introduction to the structure of the Scandinavian Caledonides. The Caledonide orogen–Scandinavia and related areas, 1, 55-68.

Roufosse, M. C. (1987). The formation and evolution of sedimentary basins in the Western Barents Sea. In Conference on petroleum geology of North West Europe. 3 (pp. 1149-1161).

Sales, J. K. (1997). Seal strength vs. trap closure-a fundamental control on the distribution of oil and gas. Seals, traps, and the petroleum system.

Serov, P., Vadakkepuliyambatta, S., Mienert, J., Patton, H., Portnov, A., Silyakova, A., ... & Hubbard, A. (2017). Postglacial response of Arctic Ocean gas hydrates to climatic amelioration. Proceedings of the National Academy of Sciences, 114(24), 6215-6220. DOI: https://doi.org/10.1073/pnas.1619288114

Schlömer, S., & Krooss, B. M. (1997). Experimental characterisation of the hydrocarbon sealing efficiency of cap rocks. Marine and Petroleum Geology, 14(5), 565-580. DOI: https://doi.org/10.1016/S0264-8172(97)00022-6

Smelror, M., Petrov, O. V., Larssen, G. B., & Werner, S. C. (2009). Geological history of the Barents Sea. Norges Geol. undersøkelse, 1-135.

Solheim, A., & Elverhøi, A. (1993). Gas-related sea floor craters in the Barents Sea. Geo-Marine Letters, 13(4), 235-243. DOI: https://doi.org/10.1007/BF01207753

Spencer, A. M., Briskeby, P. I., Christensen, L. D., Foyn, R., Kjølleberg, M., Kvadsheim, E., Knight, I., Rye-Larsen, M., & Williams, J. (2008). Petroleum geoscience in Norden-exploration, production and organization. Episodes, 31(1), 115-124.

Stoupakova, A. V., Henriksen, E., Burlin, Y. K., Larsen, G. B., Milne, J. K., Kiryukhina, T. A., Golynchik, P. O., Bordunov, S. I., Ogarkova, M. P., & Suslova, A. A. (2011). The geological evolution and hydrocarbon potential of the Barents and Kara shelves. Geological Society, London, Memoirs, 35(1), 325-344. DOI: https://doi.org/10.1144/M35.21

Sweeney, J. J., & Burnham, A. K. (1990). Evaluation of a simple model of vitrinite reflectance based on chemical kinetics. AAPG bulletin, 74(10), 1559-1570. DOI: https://doi.org/10.1306/0C9B251F-1710-11D7-8645000102C1865D

Tasianas, A., Martens, I., Bünz, S., & Mienert, J. (2016). Mechanisms initiating fluid migration at Snøhvit and Albatross fields, Barents Sea. arktos, 2(1), 1-18. DOI: https://doi.org/10.1007/s41063-016-0026-z

Tissot, B. P. & Welte D. H. (1984). Petroleum Formation and Occurrence. Springer-Verlag, Berlin, second edition.

Vadakkepuliyambatta, S., Chand, S., & Bünz, S. (2017). The history and future trends of ocean warming- induced gas hydrate dissociation in the SW Barents Sea. Geophysical Research Letters, 44(2), 835-844. DOI: https://doi.org/10.1002/2016GL071841

Vorren, T. O., Richardsen, G., Knutsen, S. M., & Henriksen, E. (1991). Cenozoic erosion and sedimentation in the western Barents Sea. Marine and petroleum geology, 8(3), 317-340. DOI: https://doi.org/10.1016/0264-8172(91)90086-G

Vorren, T. O., Hald, M., & Lebesbye, E. (1988). Late cenozoic environments in the Barents Sea. Paleoceanography, 3(5), 601-612.

Yuan, Y. S., Fan, M., Liu, W. X., Li, S. J., & Wo, Y. J. (2011). Several discussions of sealing capacity studies of caprock. Petroleum Geology & Experiment, 33(4), 336-339.

Waage, M., Portnov, A., Serov, P., Bünz, S., Waghorn, K. A., Vadakkepuliyambatta, S., Mienert, J., & Andreassen, K. (2019). Geological controls on fluid flow and gas hydrate pingo development on the Barents Sea margin. Geochemistry, Geophysics, Geosystems, 20(2), 630-650.

Waage, M., Serov, P., Andreassen, K., Waghorn, K. A., & Bünz, S. (2020). Geological controls of giant crater development on the Arctic seafloor. Scientific Reports, 10(1), 1-12. DOI: https://doi.org/10.1038/s41598-020-65018-9

Wygrala, B. (1989). Integrated study of an oil field in the southern Po basin, northern Italy (No. FZJ-2014-03033). Publikationen vor 2000.

Appendix A. This data describes timing of the Quaternary glacial cycles assigned for basin modeling.

Table A1. Determined periods of glacial cycles. From 0.12 till 0.00 Ma – determined on the basis of the UiT ice sheet model, from 2.61 till 0.12 Ma – determined on the basis of the $\delta^{18}O$ curve (Lisiecki, Raymo, 2005), demonstrated in Figure 3 in the main text of the article. MIS stands for the marine isotopic stage corresponding to time of maximum ice sheet extension during each glacial cycle. All time values are rounded to 0.01 Ma (maximum time resolution of the PetroMod software).

Glacial cycle no.	MIS	Ice growth, Ma	Ice retreat, Ma	Interglacial, Ma
1	104	2.61-2.60	2.60-2.59	2.59-2.54
2	100	2.54-2.53	2.53-2.52	2.52-2.50
3	98	2.50-2.49	2.49-2.48	2.48-2.45
4	96	2.45-2.43	2.43-2.42	2.42-2.37
5	92	2.37-2.36	2.36-2.35	2.35-2.30
6	88	2.30-2.29	2.29-2.28	2.28-2.25
7	86	2.25-2.24	2.24-2.23	2.23-2.21
8	84	2.21-2.20	2.20-2.19	2.19-2.17
9	82	2.17-2.16	2.16-2.15	2.15-2.09
10	78	2.09-2.07	2.07-2.06	2.06-2.02
11	76	2.02-2.01	2.01-2.00	2.00-1.97
12	74	1.97-1.95	1.95-1.94	1.94-1.91
13	72	1.91-1.90	1.90-1.89	1.89-1.87
14	70	1.87-1.86	1.86-1.85	1.85-1.80
15	64	1.80-1.79	1.79-1.78	1.78-1.76
16	62	1.76-1.75	1.75-1.74	1.74-1.72
17	60	1.72-1.71	1.71-1.69	1.69-1.67
18	58	1.67-1.65	1.65-1.64	1.64-1.63

19	56	1.63-1.62	1.62-1.61	1.61-1.58
20	54	1.58-1.57	1.57-1.56	1.56-1.55
21	52	1.55-1.54	1.54-1.53	1.53-1.52
22	50	1.52-1.50	1.50-1.49	1.49-1.46
23	48	1.46-1.45	1.45-1.44	1.44-1.42
24	46	1.42-1.41	1.41-1.40	1.40-1.38
25	44	1.38-1.37	1.37-1.36	1.36-1.35
26	42	1.35-1.34	1.34-1.32	1.32-1.31
27	40	1.31-1.29	1.29-1.28	1.28-1.27
28	38	1.27-1.25	1.25-1.24	1.24-1.23
29	36	1.23-1.20	1.20-1.19	1.19-1.16
30	34-32	1.16-1.10	1.10-1.09	1.09-1.07
31	30	1.07-1.04	1.04-1.03	1.03-1.01
32	28-26	1.01-0.96	0.96-0.95	0.95-0.94
33	24-22	0.94-0.87	0.87-0.86	0.86-0.84
34	20	0.84-0.80	0.80-0.79	0.79-0.77
35	18	0.77-0.72	0.72-0.70	0.70-0.69
36	16	0.69-0.63	0.63-0.62	0.62-0.61
37	14	0.61-0.54	0.54-0.50	0.50-0.48
38	12	0.48-0.43	0.43-0.42	0.42-0.39
39	10	0.39-0.34	0.34-0.33	0.33-0.31
40	8	0.31-0.25	0.25-0.24	0.24-0.20
41	6	0.20-0.14	0.14-0.13	0.13-0.10
42	5b	0.10-0.09	0.09-0.08	0.08-0.07
43	4	0.07-0.06	0.06-0.05	0.05-0.03

44	2	0.03-0.02	0.02-0.01	0.01-0.00

Appendix B. This data describes properties of the faults in the Quaternary, assigned for basin modeling. Closed – non-conductive for fluids, open – conductive for fluids.

Table B1. Properties of faults assigned for Scenario 1.

Period no.	**Age from, Ma**	**Age to, Ma**	**Type**
1	2.61	0.96	Closed
2	0.96	0.95	Open
3	0.95	0.87	Closed
4	0.87	0.86	Open
5	0.86	0.80	Closed
6	0.80	0.79	Open
7	0.79	0.72	Closed
8	0.72	0.70	Open
9	0.70	0.63	Closed
10	0.63	0.62	Open
11	0.62	0.54	Closed
12	0.54	0.50	Open
13	0.50	0.43	Closed
14	0.43	0.42	Open
15	0.42	0.34	Closed
16	0.34	0.33	Open
17	0.33	0.25	Closed
18	0.25	0.24	Open
19	0.24	0.14	Closed

20	0.14	0.13	Open
21	0.13	0.09	Closed
22	0.09	0.08	Open
23	0.08	0.06	Closed
24	0.06	0.05	Open
25	0.05	0.02	Closed
26	0.02	0.01	Open
27	0.01	0.00	Closed

953

954 **Table B2.** Properties of faults assigned for Scenario 10.

Period no.	Age from, Ma	Age to, Ma	Type
1	2.61	2.60	Closed
2	2.60	2.59	Open
3	2.59	2.53	Closed
4	2.53	2.52	Open
5	2.52	2.49	Closed
6	2.49	2.48	Open
7	2.48	2.43	Closed
8	2.43	2.42	Open
9	2.42	2.36	Closed
10	2.36	2.35	Open
11	2.35	2.29	Closed
12	2.29	2.28	Open
13	2.28	2.24	Closed
14	2.24	2.23	Open

15	2.23	2.20	Closed
16	2.20	2.19	Open
17	2.19	2.16	Closed
18	2.16	2.15	Open
19	2.15	2.07	Closed
20	2.07	2.06	Open
21	2.06	2.01	Closed
22	2.01	2.00	Open
23	2.00	1.95	Closed
24	1.95	1.94	Open
25	1.94	1.90	Closed
26	1.90	1.89	Open
27	1.89	1.86	Closed
28	1.86	1.85	Open
29	1.85	1.79	Closed
30	1.79	1.78	Open
31	1.78	1.75	Closed
32	1.75	1.74	Open
33	1.74	1.71	Closed
34	1.71	1.69	Open
35	1.69	1.65	Closed
36	1.65	1.64	Open
37	1.64	1.62	Closed
38	1.62	1.61	Open
39	1.61	1.57	Closed

40	1.57	1.56	Open
41	1.56	1.54	Closed
42	1.54	1.53	Open
43	1.53	1.50	Closed
44	1.50	1.49	Open
45	1.49	1.45	Closed
46	1.45	1.44	Open
47	1.44	1.41	Closed
48	1.41	1.40	Open
49	1.40	1.37	Closed
50	1.37	1.36	Open
51	1.36	1.34	Closed
52	1.34	1.32	Open
53	1.32	1.29	Closed
54	1.29	1.28	Open
55	1.28	1.25	Closed
56	1.25	1.24	Open
57	1.24	1.20	Closed
58	1.20	1.19	Open
59	1.19	1.10	Closed
60	1.10	1.09	Open
61	1.09	1.04	Closed
62	1.04	1.03	Open
63	1.03	0.96	Closed
64	0.96	0.95	Open

65	0.95	0.87	Closed
66	0.87	0.86	Open
67	0.86	0.80	Closed
68	0.80	0.79	Open
69	0.79	0.72	Closed
70	0.72	0.70	Open
71	0.70	0.63	Closed
72	0.63	0.62	Open
73	0.62	0.54	Closed
74	0.54	0.50	Open
75	0.50	0.43	Closed
76	0.43	0.42	Open
77	0.42	0.34	Closed
78	0.34	0.33	Open
79	0.33	0.25	Closed
80	0.25	0.24	Open
81	0.24	0.14	Closed
82	0.14	0.13	Open
83	0.13	0.09	Closed
84	0.09	0.08	Open
85	0.08	0.06	Closed
86	0.06	0.05	Open
87	0.05	0.02	Closed
88	0.02	0.01	Open
89	0.01	0.00	Closed

Highlights

Most intensive hydrocarbon leakage through open faults in Quaternary occurs during the first deglaciation event.

Apart from leaking through faults, gas is subjected to intensive capillary leakage through overburden rocks, once they reach critically small thickness during the erosion.

Gas leakage strongly depends on the total erosion thickness, the ratio between glacial and preglacial erosion thicknesses and the history of the glaciations.

Declaration of interests

☒The authors declare that they have no known competing financial interests or personal relationships that could have appeared to influence the work reported in this paper.

☐The authors declare the following financial interests/personal relationships which may be considered as potential competing interests: